University of Bath

Alternative formats
If you require this document in an alternative format, please contact:
openaccess@bath.ac.uk

Charge Scheduling for Electric Freight Vehicles

Samuel Pelletier[1], Ola Jabali[2], Gilbert Laporte[1]

[1] HEC Montréal, 3000 chemin de la Côte-Sainte-Catherine, Montréal, Canada H3C 3J7

[2] Politecnico di Milano, Piazza Leonardo da Vinci 32, 20133 Milan, Italy

e-mail addresses: {Samuel.Pelletier, Gilbert.Laporte}@hec.ca, Ola.Jabali@polimi.it

Abstract

We consider a fleet of electric freight vehicles (EFVs) that must deliver goods to a set of customers over the course of multiple days. In an urban environment, EFVs are typically charged at a central depot and rarely use public charging stations during delivery routes. Therefore, the charging schedule at the depot must be planned ahead of time so as to allow the vehicles to complete their routes at minimal cost. Vehicle fleet operators are subject to commercial electricity rate plans, which should be accounted for in order to provide an accurate estimation of the energy-related costs and restrictions. In addition, high vehicle utilization rates can accelerate battery aging, thereby requiring degradation mitigation considerations. We develop and solve a comprehensive mathematical model that incorporates a large variety of features associated with the use of EFVs. These include a realistic charging process, time-dependent energy costs, battery degradation, grid restrictions, and facility-related demand charges. Extensive numerical experiments are conducted in order to draw managerial insights regarding the impact of such features on the charging schedules of EFVs.

Keywords: electric freight vehicles, charge scheduling, green transportation, battery degradation, city logistics

1. Introduction

Electric freight vehicles (EFVs) are fast becoming a viable alternative for short- and mid-haul goods distribution (Davis and Figliozzi 2013, Lee et al. 2013, Pelletier et al. 2016, Quak et al. 2016, Franceschetti et al. 2017). Because they help reduce air and noise pollution they are often regarded as an attractive option in the context of city logistics. Most recent studies have dealt with the routing issues associated with EFVs, especially those that stem from their limited range, and have proposed models and algorithms for the optimization of routes that incorporate en route recharging (e.g., Felipe et al. 2014, Schneider et al. 2014, Bruglieri

et al. 2015, Goeke and Schneider 2015, Hiermann et al. 2016, Montoya et al. 2017). Some authors have also approached such optimization problems from a more strategic planning perspective by incorporating both routing and charging infrastructure location decisions in their models (e.g., Yang and Sun 2015, Schiffer and Walther 2017a,b,c, Schiffer et al. 2018).

The issue of depot charge scheduling for electric vehicles has received less attention than the routing component, but it nevertheless raises interesting challenges whose solution could facilitate the integration of EFVs in goods distribution schemes. Indeed, many companies using EFVs prefer charging the vehicles at their own facilities (Morganti and Browne 2018). This is due to a combination of factors, such as limited fast charging infrastructures in most regions, as well as long charging times associated with slow charging stations that lead to cargo security concerns and ineffecient use of drivers' time when charging along delivery routes (Naberezhnykh et al. 2012, Nesterova et al. 2013, E-Mobility NSR 2013). In addition, lower energy costs may be attained through commercial off-peak electricity rates when charging at the depot during specific periods of the day. Moreover, EFVs are more likely to be used in urban areas because of low driving speeds and frequent stop-and-starts, where their superior energy efficiency becomes relatively advantageous compared with that of diesel vehicles, and where financial incentives are more likely to be available. Since typical urban delivery routes are shorter than the range of currently available EFVs (Feng and Figliozzi 2013), there is often no need to consider charging outside the depot. While some studies have focused on charge scheduling for EFVs (e.g., Sassi and Oulamara 2014a,b), several important issues have not yet been addressed.

Before the publication of the recent paper by Montoya et al. (2017), charging of EFVs in a routing context was either treated as a fixed time penalty (e.g., Conrad and Figliozzi 2011, Afroditi et al. 2014, Preis et al. 2014), or was assumed to be linear with respect to time (e.g., Felipe et al. 2014, Schneider et al. 2014, Bruglieri et al. 2015, Lebeau et al. 2015, Goeke and Schneider 2015, Hiermann et al. 2016), which does not always correspond to reality. Indeed, in order to prevent overcharging the battery (i.e., operating the battery at voltage values beyond a value specified by the manufacturer), the charging function usually comprises both a linear and a non-linear component with respect to time when large charging currents are employed. Moreover, certain charging practices of electric vehicles have been shown to adversely influence the lifespan of their batteries (Bashash et al. 2011, Lunz et al. 2012). Since the battery still remains a major cost component of EFVs (Pelletier et al. 2016), it is relevant to take this consideration into account when making charge scheduling decisions. This is particularly important since high use rates have frequently been identified as a means of increasing the cost competitiveness of EFVs because of their high purchase

costs and low operational costs (Davis and Figliozzi 2013, Lee et al. 2013). However, recent studies (e.g., Taefi 2016, Taefi et al. 2016) have concluded that this may not be the case if costly battery replacements result from intensive usage in high utilization scenarios. In addition, such scenarios often involve using the vehicles in multi-shift contexts, whereby vehicles may need to perform multiple routes throughout day and night (EFVs are sometimes allowed to perform night-time deliveries in cities because they are silent, Taefi 2016). As a result, fleet operators may have to install expensive chargers at the depot in order to charge the vehicles between consecutive delivery routes during specific periods of the day, and to benefit from off-peak electricity rates. A company would probably own a limited number of chargers, typically fewer than the fleet size, thus leading to tight charging schedules. Moreover, commercial electricity rate plans are often subject to both time-dependent energy costs and facilities-related demand (FRD) charges, the latter depending on the maximum power demand registered over the course of the billing period (see, e.g., Southern California Edison, 2017). Therefore, regardless of whether the operational context requires fast chargers or not, optimizing the charging schedule can help in determining the best alternative between paying a higher FRD charge and incurring lower energy costs (e.g., by charging many vehicles when electricity is cheap), or rather keeping such FRD fees low at the expense of spreading out the charging activites throughout the day, notably when electricity is more costly.

Two relevant studies in the context of depot charge scheduling for EFVs are those of Sassi and Oulamara (2014a,b). In the first of these papers, a fleet of electric and conventional vehicles must be assigned to a set of predetermined routes so as to maximize the usage of the electric vehicles and minimize the cost of the charging schedule. Charging can only take place at the depot when the vehicles are not performing routes. The planning horizon is discretized into periods during which the charging power remains fixed and must stay within a certain interval indicating the minimum and maximum charging power of the homogeneous chargers at the depot. Charging costs and grid capacities are time-dependent. Sassi and Oulamara (2014b) have extended this problem by considering different types of chargers at the depot and a limited number of each type. They also proposed different objective functions depending on whether certain considerations are taken into account or not. These include being allowed to exceed the grid capacity by paying fixed hourly penalties, treating the number of chargers of each type at the depot as decision variables with deployment costs, and the presence of time-dependent greenhouse gas emissions costs depending on the electricity generation mix at that time.

As in Sassi and Oulamara (2014b), we focus on the depot charging schedule rather than on en route charging at public stations, but we model a more realistic charging process which

avoids overcharging, and hence battery deterioration (Lam 2011). Moreover, we work with a planning horizon of several days rather than with a single day, since the assumption that the vehicles will always be fully charged overnight does not hold in certain multi-shift operational contexts. In addition, we incorporate battery degradation considerations when determining an optimal charging schedule, as well as FRD charges. Finally, we draw several managerial insights through our numerical experiments. These relate to the impact of time-dependent energy costs, battery degradation, grid restrictions, FRD charges and **battery size** on the charging schedules of EFVs. Such insights are relatively absent from the aforementioned related studies.

The scientific aim of this paper is to model, construct and analyze charging schedules of EFVs that must operate fixed delivery routes over the course of a multiple day planning horizon in a multi-shift operational context, thereby performing several routes per day, and using vehicles that can only be charged at a central depot. With this goal in mind, Section 2 describes the problem at hand and presents a first mathematical formulation without battery degradation considerations. Section 3 explains how certain battery health considerations can be incorporated into the model. Section 4 provides extensive computational results and derives managerial insights. The paper closes with conclusions in Section 5. Appendix A contains a glossary of the abbreviations used in the paper, including those related to energy and electricity units.

2.   The EFV charge scheduling problem

The objective of this section is to introduce what we refer to as the EFV Charge Scheduling Problem (EFV-CSP). The section is organized as follows. We first provide a general description of the EFV-CSP in Section 2.1. In Section 2.2 we elaborate on the approach used to model the charging process of EFVs in discrete time. The mathematical formulation of the EFV-CSP is then given in Section 2.3, **and examples of optimal solutions for a small instance of the problem are presented in Section 2.4.** Finally, Section 2.5 provides comments on the derivation of solutions in continuous time from solutions obtained in discrete time.

As is often the case in optimization problems, several assumptions are made in the EFV-CSP, the most important of which are outlined here. First, it is assumed that the routes that must be performed by the vehicles are given but may differ from one day to another, and that the assignment of vehicles to routes is also known in advance. Working with fixed

routes simplifies the problem considerably and makes sense in multi-period routing contexts in which service consistency is valued (Kovacs et al. 2014). Note that our assumption of given routes implies that we can precompute the charge consumption a priori for each route. Second, while the charging activity of each vehicle can only occur at the depot, it can be carried out with several different chargers, i.e., we consider preemptive charging. Finally, since we formulate the EFV-CSP in discrete time, the charging schedule is determined on a period to period basis and we assume that no charging can occur during departure and arrival periods.

2.1   Problem description

The EFV-CSP is defined over a planning interval of several days which is discretized into a set $P = \{1, ..., n_p\}$ of n_p consecutive periods lasting δ hours each. The set $K = \{1, ..., m\}$ represents a fleet of m homogeneous EFVs, each equipped with a battery with a charge capacity of Q ampere-hours (Ah) and an energy capacity of E kilowatt-hours (kWh). We define the state of charge (SOC) of a battery as the amount of charge it contains divided by its maximum charge capacity Q. The set R contains all delivery routes that must be performed during the planning interval and is given as an input. Note that each vehicle may have several routes to perform. Each route $r \in R$ is associated with the following parameters: a departure period β_r, an arrival period α_r, the vehicle v_r that must perform it and the total SOC variation ΔSOC_r incurred by that vehicle. Let routes r and η_r be assigned to the same vehicle (i.e., $v_{\eta_r} = v_r$), where η_r is the route that immediately precedes route r. In other words, for each route $r \in R$, the route η_r is the route of vehicle v_r with the latest arrival period prior to β_r. Let f_k be the earliest route to be performed by vehicle k in the planning interval, and let set A_k represent all periods during which vehicle k returns from one of its routes, i.e., $A_k = \{\alpha_r | r \in R, v_r = k\}$. Assume that $\alpha_{\eta_r} = 1$ if $r = f_k$ for any vehicle $k \in K$.

At the depot, there is an energy cost of c_p in \$/kWh associated with each period $p \in P$, an FRD charge of F in \$/kW which depends on the maximum charging power retrieved from the grid throughout the planning interval, and a grid restriction G representing the maximum power in kilowatts (kW) that can be retrieved from the grid to charge the vehicles. Indeed, in addition to time-dependent energy costs and FRD fees, electricity rate plans for charging electric vehicles on company grounds may also include maximum power restrictions (see, e.g., Southern California Edison, 2017). We assume that there are different kinds of chargers installed at the depot, represented by the set S. A charger of type $s = 1$ is assumed to be a level 1 charger that comes with the vehicle upon its purchase; all vehicles can therefore use

charger $s = 1$ whenever they are at the depot. The other chargers are faster but more costly. The acquisition, installation, and maintenance costs associated with such charging equipment are significant cost components of operating electric vehicles for goods distribution (Lee et al. 2013). It is therefore assumed that a limited number $\kappa_s < m$ of chargers of type $s \in S \backslash \{1\}$ are available. As in Sassi and Oulamara (2014b), we constrain the number of charging events of the vehicles. We define a charging event as plugging a charger into a vehicle at a given time and unplugging it later. To avoid impractical solutions in which vehicles are constantly being moved from one charger to another, we set a limit of C charging events between each arrival and departure for each vehicle. The objective of the EFV-CSP is to determine a charging schedule that allows the vehicles to complete all their routes at minimal cost.

2.2   The battery charging process

Electric vehicles are typically charged under a constant current (CC)-constant voltage (CV) scheme to avoid overcharging degradation (Lam 2011). The charging current is held constant during the CC phase and the SOC thus increases linearly with respect to time since the rate of change of the SOC is charging current divided by charge capacity. During the CC phase, the terminal voltage of the battery increases until it reaches a certain maximum value V_{CV}, which is specified by the manufacturer. When it does, the CV phase begins and the terminal voltage must be maintained at that maximum value in order to avoid the degradation resulting from overcharging the battery; the charging current then decreases with time throughout the CV phase.

The process can be understood through the battery behaviour model proposed by Tremblay et al. (2007). The terminal voltage is the voltage measured at the battery terminals when it is being charged or discharged, and is a function of SOC and current. The model essentially states that the terminal voltage V_{term} of a battery is the sum of its open-circuit voltage OCV and the voltage drop across its internal resistance R, the latter term depending on the charging current $i(t)$. The open-circuit voltage is the voltage measured at the battery terminals when it is at rest and is an increasing function of SOC. Using this model, the charging terminal voltage at time t can be approximated as

$$V_{term}(SOC(t), i(t)) = OCV(SOC(t)) + R \cdot i(t). \tag{1}$$

The terminal voltage is thus larger than the open-circuit voltage during charging. During the CC phase of a CC-CV charging process, the charging current (which depends on the kind

of charger used) remains constant. As time elapses during the CC phase, the right-hand side of (1) therefore increases according to the relationship between open-circuit voltage and SOC, and hence so does the terminal voltage. As previously mentioned, the terminal voltage must never be allowed to rise above V_{CV}. Depending on the charging current used during the CC phase, V_{CV} will be reached at SOC values well below 100%. In order to continue charging the battery once V_{CV} is attained, the terminal voltage must be held at that maximum value throughout the CV phase. Following an infinitesimal time increment after entering the CV phase, the SOC will then increase according to the current in the CC phase. Since the open-circuit voltage will increase with the SOC, the current will have to be decreased in order to ensure that the terminal voltage remains at V_{CV}. The process then repeats itself following other infinitesimal time increments until the battery is fully charged.

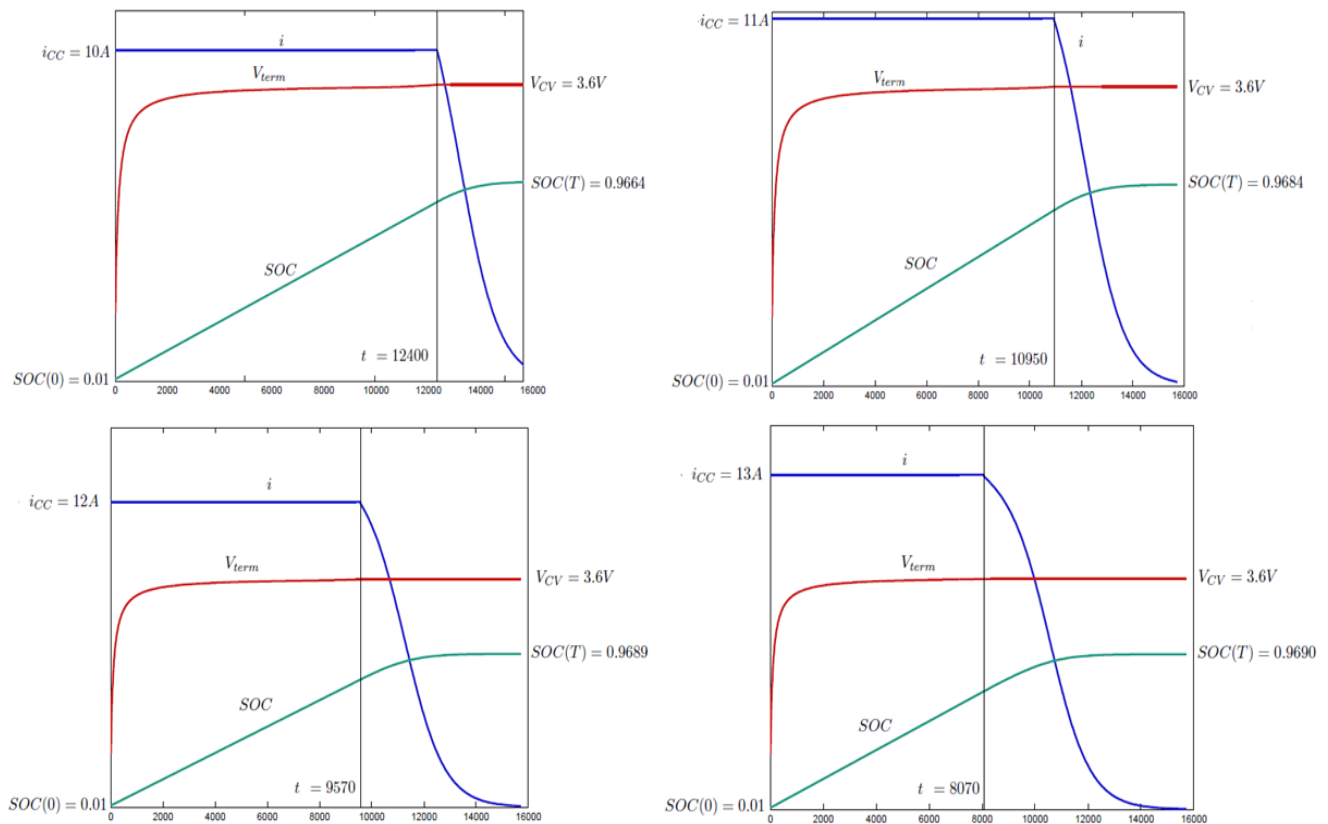Figure 1: Comparison of CC-CV charging profiles for a lithium-ion battery cell with different current values in the CC phase
Source: Pelletier et al. (2017)

Note that the charging rate used in the CC phase influences both the elapsed time and the SOC upon entering the CV phase. Indeed, a larger current will shorten the CC phase but will cause the CV phase to be entered at a lower SOC value, thereby prolonging the

CV phase. Figure 1 illustrates this process by simulating the CC-CV charging scheme for a 40Ah lithium-ion battery cell with different values for the current i_{CC} used during the CC phase and a maximum charge voltage V_{CV} of 3.6 volts (V). The final time T is set to 16,000 seconds in all the simulations. As the value of i_{CC} increases, the time t at which the CV phase is entered decreases. However, the SOC at time t is approximately 87%, 85%, 81% and 74% when i_{CC} is 10, 11, 12, and 13 amperes (A), respectively. In sum, the larger is the current used during the CC phase, the more important it is to consider the non-linear component of the charging function (e.g., for very slow chargers, a linear approximation of the entire charging function can be sufficient since the CV phase is entered at a high SOC value).

In order to model the CC-CV process in discrete time, we use a piecewise linear approximation of the evolution of SOC over time, as in Montoya et al. (2017). We assume that each charger of type $s \in S$ has a specific CC-CV charging function which is piecewise linear with $b_s + 1$ breakpoints, fitted to the real CC-CV concave function. Let a_{si} be the SOC associated with breakpoint $i \in B_s$ of the charging function of charger type s, with the set of breakpoints $B_s = \{0, ..., b_s\}$. The approximation therefore assumes that the charging current is constant between each pair of consecutive breakpoints. Let I_{si} be the charging current (A) used in the piecewise approximation between breakpoints i and $i-1$ of charger type s, for all $i \in B_s \backslash \{0\}$, with I_{s1} therefore referring to the CC phase current of charger type s.

A piecewise linear approximation of the CC-CV charging process for a charger of type s with $b_s = 3$ is illustrated in Figure 2. **This function represents how the SOC evolves with respect to time when the battery is charged with charger type s. As the figure shows, the piecewise approximation of the CC-CV process for this type of charger would have $b_s + 1 = 3 + 1 = 4$ breakpoints, represented by set $B_s = \{0, 1, 2, 3\}$. Each of these four breakpoints is associated with a specific SOC value (i.e., a_{s0}, a_{s1}, a_{s2}, and a_{s3}). Since $a_{s0} = 0$ and $a_{s4} = 1$ in this case, the figure illustrates a full charge from a SOC of zero to a SOC of one. The slope of the piecewise function between each pair of consecutive breakpoints corresponds to the charging current used between these breakpoints, divided by the battery capacity. For example, according to the definition of parameter I_{si}, I_{s2} is the charging current applied by charger type s when the SOC is between a_{s1} and a_{s2}. Thus, I_{s2}/Q corresponds to the slope of the piecewise function between these two breakpoints in Figure 2, since the charging current divided by the charge capacity is the rate of change of the SOC. Indeed, with I_{si} in amperes and the battery charge capacity Q in Ah, I_{si}/Q indicates how much the SOC will increase**

per hour when the battery is charged with a current of I_{si}.
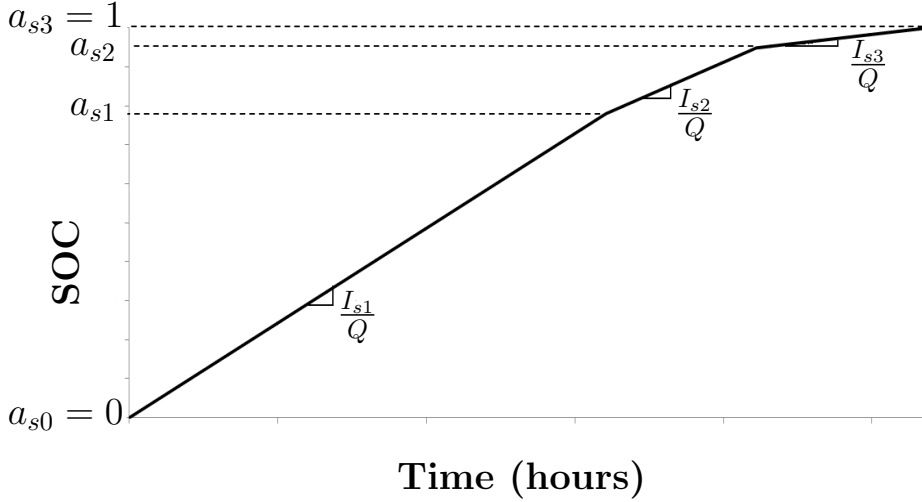
Figure 2: Piecewise linear approximation of a CC-CV charging process

Finally, note that the charging power applied to the battery during charging is equal to the product of its terminal voltage and of the charging current; it therefore increases with time during the CC phase of charging until it reaches a maximum value upon entering the CV phase, and then decreases throughout the CV phase. To ensure the respect of potential grid restrictions, let parameter P_s be the largest charging power retrieved from the grid by the battery throughout the CC-CV charging process of charger type s.

2.3 Mathematical formulation

The following decision variables are required for the formulation of the EFV-CSP without battery degradation considerations. Real and positive variables soc_{pk} refer to the state of charge of vehicle k at the start of period p, while real and positive variables i_{pk} refer to the charging current applied to vehicle k during the entirety of period p. As in Sassi and Oulamara (2014a), for modeling convenience we assume that the entire charge consumption of a route occurs during the last period of that route. For example, if vehicle $k = 1$ leaves the depot during period $p = 1$ with a SOC of 90%, and returns to the depot during period $p = 5$ with a SOC of 50%, the model is designed so that $soc_{11} = soc_{21} = soc_{31} = soc_{41} = 90\%$ and $soc_{51} = 50\%$ (so the values of soc_{pk} are irrelevant while vehicle k is performing its route; they remain the same as the departure SOC until the vehicle returns). Each vehicle starts with a given initial SOC value (i.e., soc_{1k} is a constant for each vehicle). For battery health reasons, we assume the SOC must remain between certain minimum and maximum values

SOC_{min} and SOC_{max}. The variable y indicates the maximum charging power retrieved from the grid during the planning interval.

The binary variables x_{pksi} take value 1 if vehicle k uses a charger of type s during period p with SOC values at the start and end of p between breakpoints $a_{s,i-1}$ and a_{si}, and take value 0 otherwise. It is assumed that if a charger is used by a vehicle during a period, that charger is unavailable to other vehicles for the entirety of the period. Finally, the binary variables z_{pk} take value 1 when the event of a new charge happens for vehicle k during period p, and take value 0 otherwise.

Table 1 summarizes all variable and parameter definitions discussed in this section. The following mixed integer linear programming formulation then represents the EFV-CSP:

$$\text{minimize} \quad \sum_{k \in K} \sum_{p \in P} c_p \cdot E \cdot \frac{\delta \cdot i_{pk}}{Q} + F \cdot y \tag{2}$$

subject to

$$\sum_{p=\beta_r}^{\alpha_r} \sum_{s \in S} \sum_{i \in B_s \setminus \{0\}} x_{p v_r s i} = 0 \quad r \in R \tag{3}$$

$$soc_{\alpha_r, v_r} = soc_{\beta_r, v_r} - \Delta SOC_r \quad r \in R \tag{4}$$

$$\sum_{k \in K} \sum_{i \in B_s \setminus \{0\}} x_{pksi} \leq \kappa_s \quad p \in P, s \in S \setminus \{1\} \tag{5}$$

$$\sum_{s \in S} \sum_{i \in B_s \setminus \{0\}} x_{pksi} \leq 1 \quad k \in K, p \in P \tag{6}$$

$$0 \leq i_{pk} \leq \sum_{s \in S} \sum_{i \in B_s \setminus \{0\}} I_{si} \cdot x_{pksi} \quad k \in K, p \in P \tag{7}$$

$$soc_{p+1,k} \leq a_{si} + 1 - x_{pksi} \quad k \in K, p \in P \setminus \{n_p\}, s \in S, i \in B_s \setminus \{0\} \tag{8}$$

$$soc_{pk} \geq a_{s,i-1} - 1 + x_{pksi} \quad k \in K, p \in P, s \in S, i \in B_s \setminus \{0\} \tag{9}$$

$$soc_{pk} = soc_{p-1,k} + \frac{i_{p-1,k}}{Q} \cdot \delta \quad k \in K, p \in P \setminus \{1\}, p \notin A_k \tag{10}$$

$$SOC_{min} \leq soc_{pk} \leq SOC_{max} \quad k \in K, p \in P \tag{11}$$

$$\sum_{k \in K} \sum_{s \in S} \sum_{i \in B_s \setminus \{0\}} x_{pksi} \cdot P_s \leq y \quad p \in P \tag{12}$$

$$0 \leq y \leq G \tag{13}$$

$$z_{pk} \geq \sum_{i \in B_s \setminus \{0\}} x_{pksi} - \sum_{i \in B_s \setminus \{0\}} x_{p-1,ksi} \quad k \in K, p \in P \setminus \{1\}, s \in S \tag{14}$$

Table 1: Variable and parameter definitions of the EFV-CSP model

P	Set of periods in the planning interval
K	Set of EFVs
R	Set of routes
A_k	Set of all periods during which vehicle k returns from one of its routes
S	Set of types of chargers installed at the depot
B_s	Set of breakpoints used in the piecewise linear approximation of the CC-CV charging function of charger type s
n_p	Number of periods in P
δ	Length of each period in hours
m	Number of EFVs in K
Q	Battery charge capacity (Ah)
E	Battery energy capacity (kWh)
β_r	Departure period of route r
α_r	Arrival period of route r
v_r	Vehicle that must perform route r
ΔSOC_r	Charge consumption of route r
η_r	Route of vehicle v_r with the latest arrival period prior to β_r
f_k	Earliest route to be performed by vehicle k
c_p	Energy cost during period p (\$/kWh)
F	FRD charge (\$/kW)
G	Grid restriction (kW)
κ_s	Number of chargers of type s installed at the depot
C	Maximum number of charging events between each arrival and departure for each vehicle
a_{si}	SOC associated with breakpoint $i \in B_s$ of the piecewise linear approximation of the CC-CV charging function of charger type s
I_{si}	Charging current (A) used in the piecewise linear approximation of the CC-CV charging function of charger type s between breakpoints i and $i-1$, with $i \in B_s, i > 0$
P_s	Largest charging power (kW) retrieved from the grid throughout the CC-CV charging process of charger type s
soc_{pk}	Decision variable indicating the SOC of vehicle k at the start of period p
i_{pk}	Decision variable indicating the charging current (A) applied to vehicle k during period p
y	Decision variable indicating the maximum charging power (kW) retrieved from the grid during the planning interval
x_{pksi}	Binary decision variable worth 1 if vehicle k uses a charger of type s during period p with SOC values at the start and end of p between breakpoints $a_{s,i-1}$ and a_{si}, and 0 otherwise
z_{pk}	Binary decision variable worth 1 if vehicle k begins a charge during period p, and 0 otherwise

$$z_{1k} \geq \sum_{i \in B_s \setminus \{0\}} x_{1ksi} \qquad k \in K, s \in S \tag{15}$$

$$\sum_{p=\alpha_{\eta_r}}^{\beta_r - 1} z_{pv_r} \leq C \qquad r \in R \tag{16}$$

$$x_{pksi} \in \{0, 1\} \qquad k \in K, s \in S, i \in B_s \setminus \{b_s\} \tag{17}$$

$$z_{pk} \in \{0, 1\} \qquad k \in K, p \in P. \tag{18}$$

The objective function (2) minimizes the total cost of the charging schedule. The first term corresponds to total energy costs. We conducted some numerical simulations of the CC-CV process with the battery model of Tremblay et al. (2007) and noted that the cumulative energy (kWh) recharged in the battery is fairly constant regardless of the charging current used in the CC phase, and is linear with respect to SOC during the CC-CV process. We therefore compute the SOC variation during period p of vehicle k as the charging current i_{pk} (A) multiplied by the period length δ (hours) divided by the battery charge capacity Q (Ah), and we then determine the corresponding energy recharged in the battery by multiplying the resulting SOC variation by the energy capacity E (kWh). **The second term in the objective function corresponds to the incurred FRD charges. Recall that the decision variable y indicates the maximum registered charging power retrieved from the grid over the course of the entire planning interval. Since parameter F is a fee in \$/kW which depends on the maximum charging power retrieved from the grid throughout the planning interval, the term $F \cdot y$ thus represents the incurred FRD charges.**

Constraints (3) ensure that no charging takes place while a vehicle performs its route. Constraints (4) set the SOC of each vehicle during the arrival period of each route to their SOC during the departure period of that route, minus the SOC consumption of the route. Constraints (5) state that for each charger type, at most the number of units installed of that type may be used by the fleet (these constraints are not necessary for $s = 1$). Constraints (6) force each vehicle to use at most one charger per period. Constraints (7) ensure that the charging current applied to a vehicle during a period is at most the one associated with the corresponding segment of the CC-CV charger-specific piecewise linear function. Constraints (8) and (9) appropriately bound the SOC of each vehicle at the start and end of each period depending on the CC-CV charger-specific piecewise linear function (we recall that $a_{si} \leq 1$, $\forall s \in S, i \in B_s$). Constraints (10) link the SOC of a vehicle from period $p - 1$ to period p

according the charging current used during $p-1$ (as long as p is not an arrival period for that vehicle). Constraints (11) bound the SOC of each vehicle during each period. Constraints (12) determine the maximum charging power used during the planning interval. Constraint (13) ensures that the grid restriction is respected. Constraints (14)–(16) mean that at most C new charging events take place between each arrival and departure (or between the start of the horizon and the first route if $r = f_k$). Finally, constraints (17)–(18) define the domains of the variables that are not already appropriately bounded by the other constraints. Note that variables z_{pk} can also be treated as continuous.

2.4 Two optimal solutions to the EFV-CSP

In order to help readers better understand the problem and its mathematical formulation, we now provide examples of optimal solutions for the following small instance of the EFV-CSP. The fleet consists of $m = 2$ vehicles, the planning interval contains $n_p = 16$ periods of length $\delta = 0.5$ hours each, there are $|R| = 4$ routes to be performed, and there are $|S| = 2$ types of chargers installed at the depot. Charger type $s = 1$ comes with the vehicle (i.e., $\kappa_1 = 2$), while charger type $s = 2$ is a faster charger purchased separately; we assume there is only one charger of type $s = 2$ (i.e., $\kappa_2 = 1$). We assume that energy costs c_p are \$0.10/kWh for $p = 1, ..., 5$, \$0.25/kWh for $p = 6, ..., 10$, and \$0.40/kWh for $p = 11, ..., 16$. The FRD charge F is set to \$0.40/kW. The route parameters are given in Table 2.

Table 2: Route parameters for the numerical example

r	β_r	α_r	ΔSOC_r	v_r	η_r
1	4	6	0.45	1	–
2	6	7	0.45	2	–
3	11	12	0.30	1	1
4	14	15	0.50	2	2

For the sake of simplicity, we assume that $B_1 = B_2 = \{0, 1\}$, i.e., each type of charger has only two breakpoints and the charging function is therefore linear. Since the piecewise approximation of each charging function has only one segment, index i is fixed to one everywhere in the model, e.g., in variables x_{pksi} and parameters I_{si}. Let $I_{11} = 8$A, $I_{21} = 20$A, $P_1 = 20$kW, and $P_2 = 50$kW. With period lengths of 30 minutes (i.e., $\delta = 0.5$ hours) and a battery charge capacity of $Q = 40$Ah, each period spent charging with charger type $s = 1$ can increase the

SOC by at most $(8 \cdot 0.5)/40 = 0.10$, and each period spent charging with charger type $s = 2$ can increase the SOC by at most $(20 \cdot 0.5)/40 = 0.25$. We assume that the grid restriction G can be ignored, and we set parameter C to 1, i.e., each vehicle can be charged at most once by a single charger between each of its routes (and before leaving for its first route). Each vehicle starts with a SOC of 0.25, and we set SOC_{min} to zero and SOC_{max} to 1.0. Energy costs are computed as in objective function (2) assuming an energy capacity of $E = 80$kWh.

Tables 3 and 4 illustrate two optimal solutions to the instance described above and demonstrate different strategies to minimize total costs. The solution in Table 3 focuses on keeping the FRD charge low, while the solution in Table 4 focuses on keeping the energy costs low. Indeed, in the solution of Table 3, the FRD charge is smaller since the faster charger type $s = 2$ is never used (i.e., the rows x_{p121} and x_{p221} contain only zeros), and the two vehicles are never charged simultaneously with charger type $s = 1$ during a given period (i.e., there is no period p for which $x_{p111} = 1$ and $x_{p211} = 1$). The maximum charging power used over the entire horizon is thus kept at 20kW by spreading the charging of the vehicles over more periods, notably those when the energy costs are higher. On the other hand, in the solution of Table 4, all the charging of both vehicles occurs during the first five periods of the planning horizon when energy is at its cheapest. However, in order to charge an amount during these first five periods that will allow the vehicles to perform all their routes, the faster charger of type $s = 2$ is used during each of these periods, thus increasing the FRD charge.

2.5   Deriving an equivalent solution in continuous time from the discrete time model

In order to use an equality in constraints (10), we have allowed the charging current i_{pk} in constraints (7) of the discrete time model to be less than the value I_{si} associated with the segment of the CC-CV piecewise linear function which vehicle k is using during period p. Therefore, this may result in solutions in which certain charging events do not represent the CC-CV process in continuous time. In other words, the current could go up and down from one period to the next even if the SOC remained between the same two breakpoints. However, we mention here, as a side note, that a feasible solution that respects the CC-CV process in continuous time can always be constructed from the solution obtained in discrete time. Indeed, whenever i_{pk} does not take the maximum value it could during any period of

Table 3: Optimal solution 1: Keeping the FRD charge low

Periods:	1	2	3	4	5	6	7	8	9	10	11	12	13	14	15	16
Energy costs:	0.10	0.10	0.10	0.10	0.10	0.25	0.25	0.25	0.25	0.25	0.40	0.40	0.40	0.40	0.40	0.40
Route 1 ($v_1=1$):				———————→												
Route 2 ($v_2=2$):						————→										
Route 3 ($v_3=1$):											———————→					
Route 4 ($v_4=2$):															————→	

Vehicle 1

	1	2	3	4	5	6	7	8	9	10	11	12	13	14	15	16
x_{p111}:	1	1	0	0	0	0	1	1	1	0	0	0	0	0	0	0
x_{p121}:	0	0	0	0	0	0	0	0	0	0	0	0	0	0	0	0
i_{p1}:	8	8	0	0	0	0	8	8	8	0	0	0	0	0	0	0
soc_{p1}:	0.25	0.35	0.45	0.45	0.45	0.00	0.00	0.10	0.20	0.30	0.30	0.00	0.00	0.00	0.00	0.00
z_{p1}:	1	0	0	0	0	0	1	0	0	0	0	0	0	0	0	

Vehicle 2

	1	2	3	4	5	6	7	8	9	10	11	12	13	14	15	16
x_{p211}:	0	0	1	1	1	0	0	0	0	1	1	1	1	0	0	0
x_{p221}:	0	0	0	0	0	0	0	0	0	0	0	0	0	0	0	0
i_{p2}:	0	0	8	8	8	0	0	0	0	8	8	8	8	0	0	0
soc_{p2}:	0.25	0.25	0.25	0.35	0.45	0.55	0.10	0.10	0.10	0.10	0.20	0.30	0.40	0.50	0.00	0.00
z_{p2}:	0	0	1	0	0	0	0	0	0	1	0	0	0	0	0	0

Charging power per period (kW):	20	20	20	20	20	0	20	20	20	20	20	20	20	0	0	0

Maximum charging power used (i.e., y variable): 20kW

Energy costs ($):	21.60
FRD charge ($):	8.00
Total costs ($):	29.60

Table 4: Optimal solution 2: Keeping the energy costs low

Periods:	1	2	3	4	5	6	7	8	9	10	11	12	13	14	15	16
Energy costs:	0.10	0.10	0.10	0.10	0.10	0.25	0.25	0.25	0.25	0.25	0.40	0.40	0.40	0.40	0.40	0.40
Route 1 ($v_1=1$):				———————→												
Route 2 ($v_2=2$):						————→										
Route 3 ($v_3=1$):											———————→					
Route 4 ($v_4=2$):															————→	

Vehicle 1

	1	2	3	4	5	6	7	8	9	10	11	12	13	14	15	16
x_{p111}:	0	0	0	0	0	0	0	0	0	0	0	0	0	0	0	0
x_{p121}:	1	1	0	0	0	0	0	0	0	0	0	0	0	0	0	0
i_{p1}:	20	20	0	0	0	0	0	0	0	0	0	0	0	0	0	0
soc_{p1}:	0.25	0.50	0.75	0.75	0.75	0.30	0.30	0.30	0.30	0.30	0.30	0.00	0.00	0.00	0.00	0.00
z_{p1}:	1	0	0	0	0	0	0	0	0	0	0	0	0	0	0	

Vehicle 2

	1	2	3	4	5	6	7	8	9	10	11	12	13	14	15	16
x_{p211}:	0	0	0	0	0	0	0	0	0	0	0	0	0	0	0	0
x_{p221}:	0	0	1	1	1	0	0	0	0	0	0	0	0	0	0	0
i_{p2}:	0	0	20	20	16	0	0	0	0	0	0	0	0	0	0	0
soc_{p2}:	0.25	0.25	0.25	0.50	0.75	0.95	0.50	0.50	0.50	0.50	0.50	0.50	0.50	0.50	0.00	0.00
z_{p2}:	0	0	1	0	0	0	0	0	0	0	0	0	0	0	0	0

Charging power per period (kW):	50	50	50	50	50	0	0	0	0	0	0	0	0	0	0	0

Maximum charging power used (i.e., y variable): 50kW

Energy costs ($):	9.60
FRD charge ($):	20.00
Total costs ($):	29.60

a charging event, the same SOC variation from that charging event can be obtained within less time with the CC-CV process in continuous time. Moreover, energy plans involve a few fixed rates over the course of a full day, so the function of energy costs with respect to time during a charging event is always a step function. Assuming a solution within which i_{pk} does not always take the maximum value it could during a charging event, then the same energy costs as those in the discrete time solution can be obtained with the CC-CV process in continuous time for that charging event by disconnecting and reconnecting the cable at most the number of times the step function increases and subsequently decreases. Therefore, as long as the step function representing energy costs with respect to time during a charging event is quasiconvex, the same energy costs as those in the discrete time solution can be obtained in continuous time for that charging event without having to split it into multiple events (i.e., without disconnecting and reconnecting the charging cable at some point).

Since most energy plans involve two or three rates over the course of a full day (e.g., mid-peak in the morning, peak during the afternoon, mid-peak in the evening, off-peak at night, with peak rate > mid-peak rate > off-peak rate), it seems unlikely that the function of energy costs with respect to time will increase and subsequently decrease more than once during a charging event. For example, Figure 3 illustrates the time-dependent energy costs of a rate plan offered by Southern California Edison (2017). With this plan, a charging event would need to last more than 24 hours for the step function of energy costs to increase and subsequently decrease more than once during the charging event. In addition, some charger manufacturers (e.g., eMotorWerks, 2017) have even started to offer products allowing to stop and restart charging at specific times without having to unplug and plug the cable. In this case the same energy costs can be obtained in continuous time regardless of the shape of the energy costs function with respect to time during the charging event.
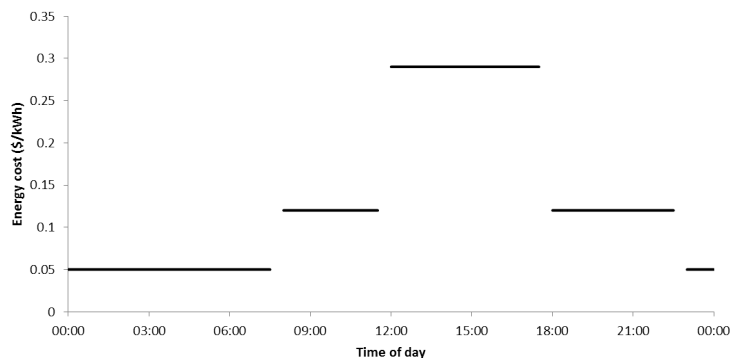

Figure 3: Example of time-dependent energy costs
Source: Southern California Edison (2017)

Finally, since the grid-related constraints (12)–(13) are modeled assuming the maximum charging power of each charger, the derived solution in continuous time will always respect the grid restriction and entail an FRD charge that is at most the one incurred in the discrete time solution.

3. Incorporating battery degradation considerations

Degradation occurs in electric vehicle batteries because of chemical and mechanical processes which ultimately lead to capacity and power fade (Barré et al. 2013). The degradation that occurs while cycling (i.e., charging or discharging) the battery is referred to as cyclic aging, while the degradation that occurs during storage is referred to as calendar aging. Battery degradation can either be estimated by using principles of electrochemistry, thereby modeling the reactions causing degradation within the battery, or by using a more empirical approach to predict battery aging according to experimental data (Bashash et al. 2011). Most transportation scientists would likely prefer a battery degradation model that can be understood without an expertise in electrochemisty and can be calibrated with easily obtainable battery specifications. Moreover, it seems desirable to use a model that transforms battery degradation directly into monetary battery wear costs. For these reasons, we propose using the model of Han et al. (2014) to take cyclic aging into account. This model uses an empirical approach to translate cyclic aging into monetary values and was applied in a vehicle-to-grid optimization problem solved with particle swarm optimization in the original paper. In Section 3.1 we detail the cyclic aging model as well as how to incorporate it into the EFV-CSP, and then in Section 3.2 we propose an intuitive approach to mitigate calendar aging when necessary via a second optimization phase.

3.1 Cyclic aging

Han et al. (2014) proposed a function representing wear costs per unit of energy going in or out of the battery according to the battery's SOC. This allows accounting for different degradation rates occurring at different SOC values. The proposed model requires the following inputs: the battery's acquisition cost, as well as its cycle life versus depth of discharge (DOD) data. The DOD indicates the amount of electrical charge discharged and charged, divided by the maximum charge capacity of the battery, e.g., a DOD of 0.3 means that the SOC of the battery has increased or decreased by 0.3 depending on whether it was being charged or discharged. The cycle life versus DOD data typically provided by battery manufacturers

indicates how many times the battery can be discharged and charged at that DOD before it reaches the end of its lifetime, assuming the battery is always discharged starting from a SOC of 1.0. Han et al. (2014) refer to this information as the Achievable Cycle Count and express it as a function of DOD (ACC-DOD). Let the function $ACC(DOD)$ refer to the ACC-DOD curve, i.e., $ACC(DOD)$ indicates how many times the battery can be discharged from a SOC of 1.0 to a SOC of $1.0 - DOD$, and then charged back from a SOC of $1.0 - DOD$ to a SOC of 1.0. For example, $ACC(0.4)$ would indicate the number of times the battery can be discharged from a SOC of 1.0 to a SOC of 0.6 and then charged back to 1.0 before the end of its lifespan. The $ACC(DOD)$ function of the lithium-ion battery used to calibrate the wear function in Han et al. (2014) is illutrated in Figure 4, where a curve is fitted to the ten data points.
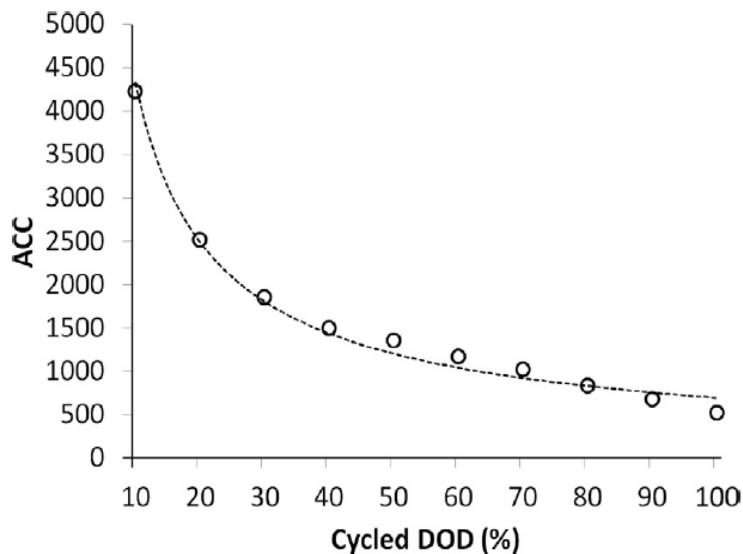

Figure 4: Illustration of $ACC(DOD)$ function for a lithium-ion battery
Source: Han et al. (2014)

However, in reality the battery will be cycled with different DOD values over its lifespan and at different starting SOC values (e.g., a DOD of 0.4 could be from 1.0 to 0.6, but also from 0.7 to 0.3, which would cause a different wear on the battery). Acknowledging this fact, Han et al. (2014) attribute a cost per kWh charged or discharged as a function of SOC based on the ACC-DOD data provided by the manufacturer. The authors propose a method for determining the wear cost function in both a continuous and a discrete manner. The discrete version can be derived as follows. A finite number of points from the ACC-DOD curve are required, and the SOC is discretized into corresponding intervals. Let $D = \{1, ..., n_d\}$ represent the set of n_d SOC intervals used to calibrate the discrete wear cost function, with

each interval $d \in D$ characterized by a lower SOC bound $\underline{S}_d$ and an upper SOC bound $\overline{S}_d$. Let L be the length of each SOC interval in D, i.e., $L = \overline{S}_d - \underline{S}_d \ \forall d \in D$. The wear cost function $W(\underline{S}_d)$ then indicates the cost per kWh charged or discharged in the SOC interval $[\underline{S}_d, \overline{S}_d]$ and satisfies

$$\text{Battery price} = 2 \cdot ACC(DOD) \cdot \sum_{d \in D: \underline{S}_d \geq 1.0 - DOD} (W(\underline{S}_d) \cdot \Delta q) \qquad DOD \in \{L, 2L, 3L, ..., 1.0\}, \quad (19)$$

where Δq is the quantity of energy (kWh) in each SOC interval. Equation (19) must hold for each value of DOD used from the ACC-DOD curve. For example, if the manufacturer's ACC-DOD curve only provides points separated by 10% DOD intervals (or if the user wants the wear cost function for SOC intervals of 10%), **then $n_d = 10$, $D = \{1, ..., 10\}$, and the lower and upper bounds of each SOC interval are given in Table 5.**

<div align="center">Table 5: SOC intervals for cyclic aging model when $n_d = 10$</div>

d	1	2	3	4	5	6	7	8	9	10
$(\underline{S}_d, \overline{S}_d)$	(0.0, 0.1)	(0.1, 0.2)	(0.2, 0.3)	(0.3, 0.4)	(0.4, 0.5)	(0.5, 0.6)	(0.6, 0.7)	(0.7, 0.8)	(0.8, 0.9)	(0.9, 1.0)

Since the length of each interval is then $L = 0.1$, expression (19) yields 10 equations, i.e., one per $DOD \in \{0.1, 0.2, ..., 1.0\}$. By isolating the wear costs $W(\underline{S}_d)$ in each of these, the following 10 equations can then be used to calibrate the wear cost function:

$$
\begin{aligned}
W(0.9) &= \frac{\text{Battery price}}{ACC(0.1) \cdot 2 \cdot \Delta q} \\
W(0.8) + W(0.9) &= \frac{\text{Battery price}}{ACC(0.2) \cdot 2 \cdot \Delta q} \\
&\vdots \\
W(0) + ... + W(0.9) &= \frac{\text{Battery price}}{ACC(1.0) \cdot 2 \cdot \Delta q}.
\end{aligned}
$$

We note that while the $ACC(DOD)$ curve is decreasing with respect to the DOD for any type of battery, the wear cost function is not necessarily increasing with the SOC. This is due to the computation in Equation (19), which does not exclusively depend on $ACC(DOD)$. The wear cost function used by Han et al. (2014) increases with the SOC, which means that cycling the battery in higher SOC intervals is more detrimental to the battery than in lower SOC intervals. We propose methodologies for incorporating monotonically increasing, monotonically decreasing and general wear costs functions with respect to SOC. Since all

wear cost functions used in our numerical experiments are monotonic, for the sake of brevity we only describe the methodology for incorporating monotonic wear cost functions in what follows. However, in Appendix B we also propose a formulation that incorporates general wear cost functions into the EFV-CSP.

In the case of monotonically increasing or decreasing wear costs with respect to SOC, the following formulation can be used to incorporate degradation costs into the EFV-CSP. As mentioned above, let $D = \{1, ..., n_d\}$ represent the set of n_d SOC intervals used to calibrate the discrete wear cost function, with interval $d \in D$ characterized by lower SOC bound $\underline{S}_d$ and upper SOC bound $\overline{S}_d$. The length of all the intervals is L, i.e., $L = \overline{S}_d - \underline{S}_d \quad \forall d \in D$. Let W_d be the wear cost per kWh charged and discharged in the SOC interval d (computed through equations (19)).

Define real variables soc_{dr}^+ as the quantity of SOC interval $d \in D$ charged into vehicle v_r between arriving from route η_r (or the start of the horizon if $r = f_{v_r}$) and leaving for route r. The binary variables u_{dr} must take a value of 1 if interval d is used to charge vehicle v_r between arriving from route η_r (or the start of the horizon if $r = f_{v_r}$) and leaving for route r (i.e., if $soc_{dr}^+ > 0$, then $u_{dr} = 1$). Note that several intervals in D can be used to charge all vehicles between two routes. Then the following constraints need to be added to the EFV-CSP regardless of whether the wear cost function is non-decreasing or non-increasing:

$$\sum_{d \in D} soc_{dr}^+ = soc_{\beta_r, v_r} - soc_{\alpha_{\eta_r}, v_r} \quad r \in R \tag{20}$$

$$0 \leq soc_{dr}^+ \leq L \cdot u_{dr} \quad d \in D, r \in R. \tag{21}$$

$$u_{dr} \in \{0, 1\} \quad d \in D, r \in R. \tag{22}$$

Constraints (20) ensure that for each vehicle, the total energy charged over all SOC intervals in D between arriving from a route and leaving for its next route is equal to the total SOC variation resulting from charging the vehicle between arriving from the preceding route and leaving for the next. Constraints (21) state that the amount of energy used in each SOC interval is at most L if that interval is allowed to be used, and 0 otherwise.

If the wear function is non-decreasing with respect to SOC, then more degradation is incurred by cycling the battery in higher SOC intervals. The following constraints should thus be added to the problem in addition to constraints (20)–(22):

$$soc_{dr}^+ \leq \overline{S}_d - soc_{\alpha_{\eta_r}, v_r} + 1 - u_{dr} \quad d \in D, r \in R. \tag{23}$$

Indeed, constraints (23) ensure that the variables u_{dr} can only take a value of 1 for SOC intervals with an upper bound that is larger than the SOC of vehicle v_r upon arriving from the previous route (or its SOC at the start of the horizon if it is the vehicle's first route). Since the wear costs increase with SOC in this case, the solution yielded by the model will always automatically fill out all lower SOC intervals, the lowest admissible interval being bounded by the difference between its upper bound and the SOC of the vehicle upon arriving from its previous route, rather than by the interval length L. **Note that with a non-decreasing wear function with respect to SOC, in any optimal solution to the EFV-CSP, all the energy charged will subsequently be discharged, and any initial charge in the batteries of the vehicles will be completely discharged (assuming $\sum_{r \in R | v_r = k} \Delta SOC_r$ is greater than soc_{1k} for all $k \in K$). The objective function (2) can thus be replaced with**

$$\text{minimize} \quad \sum_{k \in K} \sum_{p \in P} c_p \cdot E \cdot \frac{\delta \cdot i_{pk}}{Q} + F \cdot y + \sum_{r \in R} \sum_{d \in D} 2 \cdot W_d \cdot E \cdot soc_{dr}^+, \tag{24}$$

in which the total cyclic degradation costs (which should also include the cyclic degradation incurred during discharging) are computed using doubled wear costs on the amount of energy charged in each SOC interval. All discharging degradation other than that associated with discharging the initial charge in the batteries is thus computed at the time of charging. Note that with objective function (24), the initial charge in the batteries of the vehicles will still be completely discharged in any optimal solution.

On the other hand, if the wear cost function is non-increasing with respect to SOC, then more degradation is incurred by cycling the battery in lower SOC values. In this case, it is possible that some energy will be charged in an EFV-CSP optimal solution with the sole purpose of reaching (and subsequently staying in) more desirable SOC intervals. Therefore, some energy could be charged that will never be discharged, and the initial charge in the vehicles' batteries will not necessarily be completely discharged. As a result, we must compute the charging and discharging cyclic degradation separately, and thus monitor the amount of energy charged and discharged in each SOC interval of the degradation model separately as well. To this end, we use two other sets of variables in addition to variables soc_{dr}^+ and u_{dr}. Define real variables soc_{dr}^- as the quantity of SOC interval $d \in D$ discharged by vehicle v_r during route r. The binary variables π_{dr} must take a value of 1 if interval d is used to discharge the battery of vehicle v_r during

route r (i.e., if $soc_{dr}^{-} > 0$, then $\pi_{dr} = 1$). The following constraints should be then added to the problem in addition to constraints (20)–(22):

$$soc_{dr}^{+} \leq soc_{\beta_r, v_r} - \underline{S}_d + 1 - u_{dr} \quad d \in D, r \in R \tag{25}$$

$$soc_{dr}^{-} \leq soc_{\beta_r, v_r} - \underline{S}_d + 1 - \pi_{dr} \quad d \in D, r \in R \tag{26}$$

$$\sum_{d \in D} soc_{dr}^{-} = \Delta SOC_r \quad r \in R \tag{27}$$

$$0 \leq soc_{dr}^{-} \leq L \cdot \pi_{dr} \quad d \in D, r \in R \tag{28}$$

$$\pi_{dr} \in \{0, 1\} \quad d \in D, r \in R. \tag{29}$$

Indeed, in this case the model will always try to fill out all higher SOC intervals first. For charging, constraints (25) bound the highest admissible interval by the difference between its lower bound and the departure SOC of the upcoming route rather than by the interval length L; constraints (26) do the same, but for discharging (i.e., the admissible SOC intervals discharged by a vehicle during a route must have a lower bound inferior or equal to the departure SOC). Constraints (27) ensure that for each vehicle, the total energy discharged over all SOC intervals in D during route r is equal to the total SOC variation resulting from performing route r. Constraints (28) state that the amount discharged in each SOC interval is at most L if that interval is allowed to be used, and **0** otherwise. Finally, the objective function (2) should be replaced with

$$\text{minimize} \quad \sum_{k \in K} \sum_{p \in P} c_p \cdot E \cdot \frac{\delta \cdot i_{pk}}{Q} + F \cdot y + \sum_{r \in R} \sum_{d \in D} W_d \cdot E \cdot (soc_{dr}^{+} + soc_{dr}^{-}). \tag{30}$$

3.2   Calendar aging

The degradation occurring while the battery is stored always worsens with the increase in SOC. Lunz et al. (2012) showed that significant lifetime savings can be attained by charging electric vehicles as closely as possible to their departure times in order to avoid spending lengthy periods of time in higher SOC values. Although there exist some calendar aging models translating storage degradation in monetary terms that would easily lend themselves to problems akin to the EFV-CSP with periodic SOC variables, these rely on extensive long-term experimental data (e.g., Hoke et al. 2011) that may not be readily available for any given battery. Nevertheless, it would be desirable to at least mitigate calendar aging whenever

possible without overly affecting the quality of the solution obtained without calendar aging considerations. Such a mitigation is especially desired if the cycling wear cost function is non-increasing with respect to SOC, since in this case the cycling aging model would be encouraged to keep the battery in high SOC intervals. Indeed, solely considering cyclic aging does not account for the time aspect of calendar aging, e.g., charging as closely as possible to departure times is preferable from a calendar aging perspective but makes no difference from a cyclic aging perspective.

One intuitive approach to mitigate calendar life aging in the EFV-CSP is to optimize the charging schedule in two phases: first by minimizing energy, FRD and cycling degradation costs, and then by minimizing the sum of the periodic SOC variables while constraining the aforementioned total costs or individual cost components to remain the same as (or within a maximum violation of) the values found in the first phase. This should encourage the model to avoid keeping the batteries in high SOC values for lengthy periods when this can be avoided and thus take into account both the SOC and time aspects of calendar aging.

4. Computational experiments and managerial insights

We have performed an extensive computational study in order to assess the impact of different cost components in the formulation and to gain managerial insights into the proposed problem. More precisely, the aims of our experiments are: (1) to validate the proposed formulation, (2) to analyze the trade-off between energy, FRD and degradation costs under different scenarios, (3) to investigate the impact of the grid restriction on costs, (4) to illustrate how the model may be used to choose among different rate plans **and battery sizes**, and (5) to shed light on the importance of calendar aging considerations in certain contexts.

To this end, we have generated test instances and solved them under various scenarios. All test instances were solved using CPLEX 12.6 with a time limit of five hours and an optimality gap tolerance of 0.5%. The formulations were implemented in C++ and all experiments were conducted on a machine with eight Intel(R) Xeon(R) E7-8837 2.67 GHz processors with one TB of RAM running on Linux. The machine has 64 cores and each experiment was run using a single thread. We used a higher optimality gap tolerance than the default setting because our goal with these experiments is not to demonstrate the computational prowess of the model, but rather to derive meaningful managerial insights from reasonably good (in fact optimal or quasi-optimal) solutions. **Except for the five tests in Section 4.8, for which the second phase of the approach proposed in Section 3.2 is performed,**

the remaining 225 tests generate a solution with an optimality gap between 0% and 1.81% within the time limit. The average optimality gap of all 230 tests is 0.50%. (The worst gap for the above-mentioned five tests using the objective function of the second phase proposed in Section 3.2 is 3.35%.)

4.1   Description of the base case scenario

We have generated test instances in which the vehicles are used in a multi-shift fashion throughout the day, thereby performing two routes per 24-hour interval (we allow both day and night routes). The fleet vehicles are assumed to be medium-duty electric trucks equipped with 80kWh batteries, each consisting of several 3.2V-40Ah lithium-ion battery cells. We generated five test instances for each fleet size m of three, six and nine vehicles. The planning horizon begins at 6:00 and each vehicle is then assumed to have a SOC of 0.90. We worked with a planning horizon of three days and with period lengths of 30 minutes.

Let set $K_1 = \{1, 3, ...\}$ refer to the vehicles in K indexed by odd numbers, and let set $K_2 = \{2, 4, ...\}$ refer to the vehicles in K indexed by even numbers. For vehicles in K_1, the first route of each day occurs between 7:00 and 13:00, and the second route occurs between 19:00 and 1:00. The departure time is randomly generated between 7:00 and 9:00 for the first route, and between 19:00 and 21:00 for the second route. Similarly, the arrival time is randomly generated between 11:00 and 13:00 for the first route, and between 23:00 and 1:00 for the second route. For vehicles in K_2, the first route occurs between 12:00 and 18:00, and the second route occurs between 0:00 and 6:00, with departure and arrival times generated in a similar fashion. Davis and Figliozzi (2013), who also focus on depot charging, report that scenarios in which the daily distances traveled by electric trucks approach their maximum range can significantly help their business case. The SOC consumption of all routes is thus randomly generated between 0.4 and 0.47 so that the vehicles discharge at least 80% of their battery on a daily basis. This is a reasonable representation of double-shift usage of the vehicles, considering typical daily miles traveled by urban delivery trucks are about 40 to 50 miles (Feng and Figliozzi 2013).

Using some battery modeling considerations detailed in Pelletier et al. (2017) with battery cell parameters from Marra et al. (2012), we conducted numerical simulations of the CC-CV charging process for such battery cells with a maximum charge voltage of 3.65V and two different charging currents during the CC phase: 3.5A and 17.5A. We set SOC_{min} to 0.05 and SOC_{max} to 0.99 for battery health reasons. **We consider that the 3.5A charger corresponds to an on-board charger that comes with the vehicle upon its purchase**

(i.e., each vehicle has one), and that the 17.5A charger corresponds to a costly off-board fast charger (i.e., there are fewer 17.5A chargers than there are vehicles in the fleet). Our simulations of the CC-CV charging process indicate that approximately 600 of the considered battery cells would need to be connected to form the battery pack so that a full charge from SOC_{min} to SOC_{max} corresponds to 80kWh put into the battery, resulting in maximum charging powers of approximately 7.6kW for the 3.5A charger and 38kW for the 17.5A charger. These values are in line with maximum powers for AC level 2 (240V) slow charging and DC level 1 (600V) fast charging mentioned by Shareef et al. (2016) in their review of state-of-the-art charging technologies for electric vehicles.

With the 3.5A charger, the batteries can be fully charged from SOC_{min} to SOC_{max} in just under 11 hours. The CV process is entered at a SOC of almost 0.98, so for the sake of simplicity we approximate the entire CC-CV process with two breakpoints: 0.05 and 0.99. With the 17.5A charger, the batteries can be fully charged from SOC_{min} to SOC_{max} in just under three hours. The CV process is entered at a SOC of 0.78, and we approximate the CC-CV process associated with this charger with four breakpoints: 0.05, 0.78, 0.95, and 0.99. In all tested instances, we use a depot charging infrastructure consisting of m slow chargers (i.e., 3.5A) and $(m/3 - 1)$ fast chargers (i.e., 17.5A). **This infrastructure seems reasonable, since 1) considering the large costs associated with the acquisition, installation, and maintenance costs of fast chargers, a company would most likely want to get by with only a few (if any) of them, and 2) using several fast chargers simultaneously can potentially overload the grid, thus limiting the number of such chargers that may be installed at the depot.** We allow each vehicle to perform two charging events (i.e., $C = 2$) between each pair of consecutive routes.

We used the time-dependent energy costs offered by Southern California Edison (2017) in their TOU-EV-4 plan for businesses charging electric vehicles on company grounds. The energy prices vary with time of day and season. Peak hours are from noon to 18:00; mid-peak hours are from 8:00 to noon and from 18:00 to 23:00; and off-peak hours are from 23:00 to 8:00. Summer rates are in place from the first Saturday of June to the first Saturday of October, while winter rates apply for the rest of the year. The energy rates and FRD charge of the TOU-EV-4 plan are summarized in Table 6. With the TOU-EV-4 plan, the maximum charging power must remain under 500kW, so the grid restriction can be ignored under these circumstances. Assuming 22 working days per month, the FRD charge of $13.20/kW would be equivalent to $1.8/kW over a planning horizon of three days.

Finally, regarding battery degradation, we consider a battery wear cost function cali-

Table 6: Rates ($/kWh) and monthly FRD charge ($/kW) under the TOU-EV-4 plan

	Summer	Winter
Peak (12:00–18:00)	0.29	0.11
Mid-peak (8:00–12:00, 18:00–23:00)	0.12	0.09
Off-peak (23:00–8:00)	0.05	0.06
FRD charges	13.20	13.20

brated with the cycle life data used in the original paper of Han et al. (2014), resulting in a non-decreasing wear cost function. It is therefore preferable to avoid cycling such a battery in high SOC values. We calibrate the degradation costs for SOC intervals of 25% assuming battery costs of $410/kWh (see Nykvist and Nilsson 2015) and thus a battery price of $32,800. We also multiply the obtained wear costs by two and use objective function (24), since the wear cost function is non-decreasing. The resulting costs (i.e., $2 \cdot W_d$) are reported in Table 7.

Table 7: Battery wear cost function

SOC interval	Degradation costs
0–0.25	$0.48/kWh
0.25–0.5	$0.52/kWh
0.5–0.75	$0.58/kWh
0.75–1	$0.79/kWh

4.2   Base case results

The results for the problem setting described in Section 4.1 when all cost components (i.e., energy, degradation, and FRD) are jointly minimized are reported in Table 8. We also present in Table 9 the results obtained when only optimizing energy costs and the FRD charge. The columns "Energy (1)", "Deg. (2)" and "FRD (3)" report the obtained energy costs, degradation costs, and FRD charge, respectively. The column "Avg. SOC" reports the average SOC of the vehicles upon departing for their routes. The entries of Tables 8 and 9 show that incurring a slightly larger sum of energy costs and FRD charges can be worthwhile in order to cycle the battery in specific SOC intervals and thus lower battery degradation costs. Note that since the degradation costs used increase with SOC (see Table 7), the model tries to cycle the battery in low SOC intervals when the degradation costs are included in the optimization process, and the average departing SOC thus decreases significantly.

Whether degradation costs are jointly optimized or not, the FRD charge for a given

Table 8: Costs obtained when minimizing energy, degradation and FRD costs

Instance	Summer rates							Winter rates						
	Energy (1)	Deg. (2)	FRD (3)	Total A (1)+(3)	Avg. SOC	Total B (1)+(2)+(3)	Time (s)	Energy (1)	Deg. (2)	FRD (3)	Total A (1)+(3)	Avg. SOC	Total B (1)+(2)+(3)	Time (s)
1-3V	39.53	220.75	27.36	66.89	0.62	287.64	0.06	34.06	213.31	27.36	61.42	0.56	274.73	842.42
2-3V	33.16	216.85	27.36	60.52	0.63	277.37	0.05	32.72	207.44	27.36	60.08	0.56	267.52	1044.34
3-3V	41.42	223.62	27.36	68.78	0.60	292.40	0.06	34.50	217.92	27.36	61.86	0.56	279.78	1424.99
4-3V	35.15	217.73	27.36	62.51	0.62	280.24	0.05	33.00	209.87	27.36	60.36	0.56	270.23	18000.00
5-3V	32.36	217.86	27.36	59.72	0.61	277.58	0.13	32.63	210.64	27.36	59.99	0.56	270.63	2512.42
1-6V	77.22	431.85	41.04	118.26	0.60	550.11	39.36	65.94	421.37	41.04	106.98	0.55	528.35	18000.00
2-6V	58.03	424.42	68.40	126.43	0.57	550.85	10.17	66.69	420.32	41.04	107.73	0.55	528.05	18000.00
3-6V	79.64	430.66	41.04	120.68	0.59	551.34	97.20	66.03	421.17	41.04	107.07	0.56	528.24	18000.00
4-6V	57.52	433.21	68.40	125.92	0.58	559.13	15.25	67.36	428.78	41.04	108.40	0.56	537.18	18000.00
5-6V	58.85	424.31	68.40	125.25	0.57	551.56	7.54	66.80	422.24	41.04	107.84	0.56	530.08	9663.27
1-9V	107.16	648.43	68.40	175.56	0.59	823.99	511.50	103.02	636.18	54.72	157.74	0.56	793.92	152.39
2-9V	109.18	648.34	68.40	177.58	0.59	825.92	125.38	103.11	635.81	54.72	157.83	0.56	793.64	242.75
3-9V	104.29	652.96	68.40	172.69	0.60	825.65	20.56	104.72	637.79	54.72	159.44	0.56	797.23	238.08
4-9V	97.38	656.60	82.08	179.46	0.59	836.06	95.77	105.02	646.43	54.72	159.74	0.56	806.17	185.05
5-9V	96.27	661.93	82.08	178.35	0.59	840.28	9.43	104.72	650.94	54.72	159.44	0.56	810.38	357.57

Table 9: Costs obtained when minimizing energy and FRD costs

Instance	Summer rates							Winter rates						
	Energy (1)	Deg. (2)	FRD (3)	Total A (1)+(3)	Avg. SOC	Total B (1)+(2)+(3)	Time (s)	Energy (1)	Deg. (2)	FRD (3)	Total A (1)+(3)	Avg. SOC	Total B (1)+(2)+(3)	Time (s)
1-3V	32.38	250.46	27.36	59.74	0.76	310.20	0.06	35.83	249.22	13.68	49.51	0.74	298.73	0.06
2-3V	31.04	239.84	27.36	58.40	0.73	298.24	0.16	34.71	237.17	13.68	48.39	0.72	285.56	0.08
3-3V	35.43	241.39	27.36	62.79	0.70	304.18	0.08	36.89	252.42	13.68	50.57	0.74	302.99	0.10
4-3V	31.46	237.77	27.36	58.82	0.71	296.59	0.12	35.20	242.71	13.68	48.88	0.72	291.59	0.04
5-3V	30.43	241.53	27.36	57.79	0.71	299.32	0.55	34.81	239.81	13.68	48.49	0.70	288.30	0.11
1-6V	68.24	472.83	41.04	109.28	0.70	582.11	141.43	69.91	484.67	27.36	97.27	0.72	581.94	36.21
2-6V	69.30	478.72	41.04	110.34	0.71	589.06	119.27	70.20	495.01	27.36	97.56	0.74	592.57	189.57
3-6V	68.53	480.48	41.04	109.57	0.71	590.05	56.58	69.67	488.21	27.36	97.03	0.72	585.24	89.35
4-6V	70.17	499.46	41.04	111.21	0.74	610.67	77.03	71.41	503.71	27.36	98.77	0.75	602.48	107.36
5-6V	69.44	492.97	41.04	110.48	0.74	603.45	161.81	70.44	492.92	27.36	97.80	0.74	590.72	214.44
1-9V	97.67	711.91	68.40	166.07	0.70	877.98	271.57	105.67	753.72	41.04	146.71	0.75	900.43	257.68
2-9V	97.46	698.27	68.40	165.86	0.68	864.13	219.74	105.85	736.89	41.04	146.89	0.73	883.78	98.70
3-9V	98.95	728.59	68.40	167.35	0.72	895.94	227.92	106.79	749.34	41.04	147.83	0.74	897.17	246.34
4-9V	99.42	714.88	68.40	167.82	0.70	882.70	52.68	107.77	749.39	41.04	148.81	0.73	898.20	424.69
5-9V	100.53	726.73	68.40	168.93	0.70	895.66	7649.27	108.70	760.81	41.04	149.74	0.74	910.55	103.11

instance solved with the summer rates is always at least equal to the FRD charge for the same instance solved with the winter rates. This outcome is a result of the very high peak energy costs of the summer rates. With the winter rates, peak rates are sufficiently low to charge vehicles during peak hours and thus keep FRD charges lower by spreading out charging of vehicles over larger time intervals. On the other hand, with the summer rates, vehicles are rarely charged during peak hours in order to avoid very high peak rates, thereby requiring one to charge more vehicles simultaneously or the use of faster chargers retrieving more power from the grid when energy is cheap, and thus incurring higher FRD charges.

4.3   The impact of facility-related demand charges

Although the FRD charge makes the problem significantly harder to solve, ignoring it may lead to undesirable solutions. To demonstrate this, we solved the test instances described in Section 4.1 by only optimizing energy and degradation costs. The results are presented in Table 10 and show how disregarding the FRD charge when optimizing the charging schedule leads to solutions in which the decrease in energy costs (achievable by being able to charge any amount of vehicles simultaneously with any type of charger without any penalty) does not compensate for the much higher FRD charge, especially for the larger fleet sizes of six and nine vehicles. Indeed, for these instances, the obtained FRD charge in Table 10 is often larger than the sum of the energy costs and the FRD charge in Table 8, while still generating similar degradation costs.

One should also carefully consider such FRD charges when determining the depot charging infrastructure if fast chargers are not required from a feasibility perspective. Indeed, while the fast chargers are heavily used in the solutions obtained when ignoring the FRD charge (i.e., those reported in Table 10), they are often not used at all in the solutions obtained when jointly optimizing energy, degradation and FRD costs (i.e., those reported in Table 8) because of the large charging power they retrieve from the grid and the associated FRD charge. Therefore, although fast chargers certainly have their utility in certain operational contexts where they are required to allow vehicles to perform their routes (as will be shown in the next section), the notion of purchasing such fast chargers solely in order to perform the bulk of charging during specific periods of the day when energy is cheap may not be justifiable in certain contexts in the presence of FRD charges.

Table 10: Costs obtained when minimizing energy and degradation costs

Instance	Summer rates					Winter rates				
	Energy	Deg.	FRD	Total	Time (s)	Energy	Deg.	FRD	Total	Time (s)
1-3V	36.32	220.37	41.04	297.73	0.04	34.03	213.31	41.04	288.38	0.03
2-3V	31.69	214.85	41.04	287.58	0.03	32.61	207.44	41.04	281.09	0.03
3-3V	38.01	223.63	41.04	302.68	0.04	34.50	217.92	41.04	293.46	0.03
4-3V	33.02	216.45	41.04	290.51	0.04	33.00	209.87	41.04	283.91	0.03
5-3V	30.22	217.48	41.04	288.74	0.03	32.63	210.64	41.04	284.31	0.03
1-6V	54.71	425.14	136.80	616.65	0.46	57.12	422.40	136.80	616.32	0.44
2-6V	57.90	422.48	109.44	589.82	0.49	57.30	422.62	109.44	589.36	0.52
3-6V	59.93	423.39	123.12	606.44	0.49	58.30	421.59	136.80	616.69	0.42
4-6V	57.97	431.39	123.12	612.48	0.58	58.44	428.72	123.12	610.28	0.51
5-6V	58.32	422.64	123.12	604.08	0.51	57.40	424.14	123.12	604.66	0.55
1-9V	85.18	640.19	177.84	903.21	0.40	86.74	637.45	177.84	902.03	0.48
2-9V	86.16	637.98	191.52	915.66	0.45	86.81	637.34	177.84	901.99	0.70
3-9V	89.08	642.09	164.16	895.33	0.41	88.27	639.32	177.84	905.43	0.73
4-9V	89.39	646.19	205.20	940.78	0.52	87.93	649.51	205.20	942.64	0.42
5-9V	89.80	652.39	205.20	947.39	0.64	88.61	651.79	205.20	945.60	0.40

4.4 The impact of longer routes

To determine the impact of longer routes, we modified the instances described in Section 4.1 to generate two alternative scenarios. In the first, the two short routes in each 24-hour interval are merged into a single long route. While performing a single long route certainly has its logistical advantages, it also leaves much less leeway regarding the selection of SOC intervals within which to cycle the battery and thus limits cyclic aging mitigation. To generate the instances with a single long route per day, we simply merge the two routes of each vehicle into a single route, departing at the time of the earliest route, lasting the sum of the lengths of each route, and using the total SOC consumption of the two routes. Therefore, in the single long route per day scenario, all routes consume between 80% and 94% of the battery (note that 94% is the maximum feasible consumption for a route considering SOC_{min} and SOC_{max}). The results are presented in Table 11. The column "Base case"reports the total cost obtained for that instance under the base case scenario (see Table 8). The results indicate that it is indeed preferable to split the long route into two in order to avoid cycling the battery in high SOC intervals.

In the second alternative scenario with longer routes, we simply use the same routes as in the base case scenario in terms of when they occur, but we double the SOC consumption of each route. The vehicles thus perform two routes per day, each consuming between 80%

Table 11: Costs obtained when minimizing energy, degradation and FRD costs for the scenario with one longer route per day

Instance	Summer rates						Winter rates					
	Energy	Deg.	FRD	Total	Time (s)	Base case	Energy	Deg.	FRD	Total	Time (s)	Base case
1-3V	32.89	247.59	27.36	307.84	0.13	287.64	30.48	246.97	27.36	304.81	0.38	274.73
2-3V	32.03	239.61	27.36	299.00	0.05	277.37	29.82	239.61	27.36	296.79	0.10	267.52
3-3V	33.96	254.55	27.36	315.87	0.05	292.40	31.18	254.55	27.36	313.09	0.43	279.78
4-3V	33.25	243.26	27.36	303.87	0.06	280.24	30.12	243.04	27.36	300.52	1.56	270.23
5-3V	32.61	244.06	27.36	304.03	0.05	277.58	30.38	244.06	27.36	301.80	0.23	270.63
1-6V	64.26	488.36	54.72	607.34	37.26	550.11	65.02	490.68	41.04	596.74	37.38	528.35
2-6V	64.48	486.35	54.72	605.55	43.27	550.85	64.95	486.35	41.04	592.34	20.13	528.05
3-6V	64.22	487.48	54.72	606.42	28.61	551.34	64.97	489.09	41.04	595.10	23.32	528.24
4-6V	66.36	499.75	54.72	620.83	130.44	559.13	66.52	505.30	41.04	612.86	18000.00	537.18
5-6V	65.02	490.12	54.72	609.86	43.40	551.56	65.64	490.24	41.04	596.92	30.19	530.08
1-9V	97.57	737.86	82.08	917.51	18000.00	823.99	95.91	738.07	68.40	902.38	16394.65	793.92
2-9V	98.03	736.73	82.08	916.84	18000.00	825.92	96.02	736.73	68.40	901.15	77.52	793.64
3-9V	98.30	741.24	82.08	921.62	16498.00	825.65	95.90	741.24	68.40	905.54	462.54	797.23
4-9V	99.84	753.40	82.08	935.32	275.54	836.06	97.35	753.27	68.40	919.02	229.40	806.17
5-9V	100.29	758.74	82.08	941.11	16259.38	840.28	98.07	759.21	68.40	925.68	323.50	810.38

and 94% of the battery. Under this scenario, all three-vehicle instances (in which there is no fast charger) become infeasible, showing that despite their impact on FRD charges, fast chargers can be useful in high EFV utilization contexts with long routes. Indeed, the six-vehicle and nine-vehicle instances (in which there are one and two fast chargers, respectively) are feasible under this scenario and make heavy use of the fast chargers. These results are presented in Table 12. The total costs obtained for the base case scenario are also reported. It is interesting to note that although the charge consumption of the routes are doubled, the total costs are nearly tripled compared with the base case. Each individual cost component (i.e., energy, degradation and FRD) is more than doubled compared to the results from Table 8 for almost all the six- and nine-vehicle instances. Indeed, the larger charge consumption of the routes requires regularly cycling the battery in high SOC intervals (explaining the large increase in degradation costs), but also forces the model to use the fast chargers in order to allow the vehicles to perform their routes (explaining the large increase in FRD charges). This contingency in turn forces a significant amount of day-time inter-route charging to occur during peak hours due to the ratio of vehicles to fast chargers (explaining the large increase in energy costs).

Table 12: Costs obtained when minimizing energy, degradation and FRD costs for the scenario with two longer routes per day

Instance	Summer rates						Winter rates					
	Energy	Deg.	FRD	Total	Time (s)	Base case	Energy	Deg.	FRD	Total	Time (s)	Base case
1-6V	246.26	1211.46	95.76	1553.48	16207.84	550.11	172.64	1211.43	82.08	1466.15	18000.00	528.35
2-6V	245.44	1211.01	95.76	1552.21	16078.18	550.85	166.82	1209.18	95.76	1471.76	18000.00	528.05
3-6V	259.97	1211.87	95.76	1567.60	473.43	551.34	168.56	1210.69	95.76	1475.01	18000.00	528.24
4-6V	254.13	1237.57	95.76	1587.46	474.61	559.13	169.54	1235.18	95.76	1500.48	18000.00	537.18
5-6V	247.53	1216.01	95.76	1559.30	16231.25	551.56	168.69	1213.96	95.76	1478.41	18000.00	530.08
1-9V	351.02	1829.45	164.16	2344.63	1103.25	823.99	244.17	1828.40	164.16	2236.73	18000.00	793.92
2-9V	362.35	1827.63	164.16	2354.14	16246.07	825.92	246.26	1827.63	164.16	2238.05	18000.00	793.64
3-9V	364.32	1836.28	164.16	2364.76	16265.76	825.65	247.96	1834.70	164.16	2246.82	18000.00	797.23
4-9V	349.52	1861.71	164.16	2375.39	16319.24	836.06	247.82	1861.71	164.16	2273.69	18000.00	806.17
5-9V	362.45	1869.12	164.16	2395.73	16243.70	840.28	249.09	1869.12	164.16	2282.37	18000.00	810.38

4.5   The impact of the grid restriction

We now investigate the impact of maximum allowed loads on energy and degradation costs by solving the instances described in Section 4.1 with another rate plan offered by Southern California Edison (2017): TOU-EV-3-B (see Table 13). Under this plan, the maximum power retrieved from the grid must always remain below 20kW. In this case, the $7.23/kW monthly FRD fee is equivalent to approximately $0.99/kW for the three-day planning horizon, assuming once again 22 working days per month.

Table 13: Rates ($/kWh) and monthly FRD charge ($/kW) under the TOU-EV-3-B plan

	Summer	Winter
Peak (12:00–18:00)	0.33	0.12
Mid-peak (8:00–12:00, 18:00–23:00)	0.14	0.11
Off-peak (23:00–8:00)	0.06	0.07
FRD	7.23	7.23

All three-vehicle instances use a maximum charging power under 20kW with the plan TOU-EV-3-B, regardless of whether the restriction of 20kW is enforced or not, and all nine-vehicle instances are infeasible under the grid restriction of 20kW. We therefore present only the results for the six-vehicle instances under plan TOU-EV-3-B in Table 14, in which G indicates that the grid restriction of 20kW was enforced during the optimization process, and NG indicates that the grid restriction was ignored. All three cost components are jointly optimized. The most notable impact of the grid restriction is on energy costs. With the summer rates, the energy costs are nearly doubled when solving the same instance without the grid restriction and with the grid restriction of 20kW. Indeed, the grid restriction prevents

the model from taking advantage of significant savings regarding energy costs since it limits the number of vehicles that can be simultaneously charged at any given moment, namely when energy is cheaper. Although the grid restriction naturally leads to a smaller FRD charge, the increase in energy and degradation costs outweighs these savings and results in significantly higher total costs. The increase in energy costs is, however, less significant with the winter rates, since energy costs outside off-peak hours are smaller than with the summer rates. The difference in total costs obtained with and without the grid restriction is therefore quite smaller with the winter rates.

We also mention that while all the six-vehicle instances from Section 4.1 are feasible despite the grid restriction of 20kW, they are no longer feasible when modified as described in the first paragraph of Section 4.4, i.e., when the two routes of each day are merged into one long route. This suggests that binding grid restrictions can hinder high EFV utilization in the presence of long routes, and that splitting such long routes into shorter ones spread out throughout the day and night can also be beneficial with regard to vehicle operation flexibility in the presence of such grid restrictions.

Table 14: The impact of the grid restriction on costs under plan TOU-EV-3-B

Instance	Summer rates					Winter rates				
	Energy	Deg.	FRD	Total	Time (s)	Energy	Deg.	FRD	Total	Time (s)
1-6V-G	132.25	455.28	15.05	602.58	7.11	83.25	448.85	15.05	547.15	4.25
2-6V-G	133.68	459.80	15.05	608.53	3.51	83.54	454.31	15.05	552.90	3.60
3-6V-G	130.37	452.25	15.05	597.67	3.73	82.97	445.84	15.05	543.86	3.13
4-6V-G	136.39	470.10	15.05	621.54	4.54	84.77	464.72	15.05	564.54	7.93
5-6V-G	134.83	462.33	15.05	612.21	3.37	83.79	456.58	15.05	555.42	4.10
1-6V-NG	68.02	425.22	37.62	530.86	1.32	77.21	421.78	22.57	521.56	38.16
2-6V-NG	67.98	424.83	37.62	530.43	2.27	78.97	420.68	22.57	522.22	46.47
3-6V-NG	69.77	425.54	37.62	532.93	1.37	77.50	421.25	22.57	521.32	44.54
4-6V-NG	68.17	433.27	37.62	539.06	2.56	78.99	428.74	22.57	530.30	7.56
5-6V-NG	70.26	424.25	37.62	532.13	0.96	78.91	423.39	22.57	524.87	70.74

4.6 Using the model to select an energy rate plan

A desirable feature of our model is that it can be used to choose among different rate plans offering trade-offs between energy costs, FRD charges, and fixed customer charges when the operational context is compatible with the grid restriction of each option. For example, the

TOU-EV-3-B plan has higher energy costs, a lower FRD charge, and a fixed customer charge of \$0.84 per day, while the TOU-EV-4 plan has lower energy costs, a higher FRD charge, and a fixed customer charge of \$198.79 per month. Table 15 presents the costs obtained with each of the plans for the six-vehicle instances described in Section 4.1 when optimizing all cost components. The total cost also includes the fixed customer charge of \$2.52 for the TOU-EV-3-B plan (i.e., \$0.84 per day for a three day planning horizon) and of \$19.88 for the TOU-EV-4 plan (based on \$198.79 per month for a three day planning horizon, assuming 30 days per month). The TOU-EV-4 plan appears to be the best choice in this context.

Table 15: Cost comparison of the TOU-EV plan options

Instance	Summer rates					Winter rates				
	Energy	Deg.	FRD	Cus.chg	Total	Energy	Deg.	FRD	Cus.chg	Total
1-6V-TOU-EV-3-B	132.25	455.28	15.05	2.52	605.10	83.25	448.85	15.05	2.52	549.67
2-6V-TOU-EV-3-B	133.68	459.80	15.05	2.52	611.05	83.54	454.31	15.05	2.52	555.42
3-6V-TOU-EV-3-B	130.37	452.25	15.05	2.52	600.19	82.97	445.84	15.05	2.52	546.38
4-6V-TOU-EV-3-B	136.39	470.10	15.05	2.52	624.06	84.77	464.72	15.05	2.52	567.06
5-6V-TOU-EV-3-B	134.83	462.33	15.05	2.52	614.73	83.79	456.58	15.05	2.52	557.94
1-6V-TOU-EV-4	77.22	431.85	41.04	19.88	569.99	65.94	421.37	41.04	19.88	548.23
2-6V-TOU-EV-4	58.03	424.42	68.40	19.88	570.73	66.69	420.32	41.04	19.88	547.93
3-6V-TOU-EV-4	79.64	430.66	41.04	19.88	571.22	66.03	421.17	41.04	19.88	548.12
4-6V-TOU-EV-4	57.52	433.21	68.40	19.88	579.01	67.36	428.78	41.04	19.88	557.06
5-6V-TOU-EV-4	58.85	424.31	68.40	19.88	571.44	66.80	422.24	41.04	19.88	549.96

4.7 The impact of battery size

A possible way to decrease EFV purchase costs may be to acquire vehicles with a smaller battery. However, a smaller battery would need to be discharged with a larger DOD more frequently, which could accelerate its deterioration. To investigate the impact of battery size, we solved the test instances described in Section 4.1 by assuming the battery pack now contains 300 of the considered lithium-ion cells rather than 600, so that a full charge from SOC_{min} to SOC_{max} corresponds to approximately 40kWh instead of 80kWh as in all previous experiments. Using the same battery costs of \$410/kWh, the battery price thus becomes \$16,400. With the cycle life data used by Han et al. (2014) as well as the new battery price and energy capacity, the wear costs from Table 7 remain the same. Assuming the chargers described in Section 4.1 would apply the same

maximum charging powers to the smaller battery, the charging currents applied during the CC phase become 7A and 35A for the 7.6kW and 38kW chargers, respectively. The piecewise functions used to approximate the CC-CV processes are adjusted accordingly. Since the initial SOC in all previous experiments with the large 80kWh battery was set to 0.9, in order to achieve a fair comparison with the small 40kWh battery we solved the base case scenario with the large battery again but with a different initial SOC. The initial SOC is set to 0.45 for the 80kWh battery, and to 0.90 for the 40kWh battery. The results are presented in Table 16 for both the 40kWh battery and the 80kWh batery.

Table 16: Comparison of costs obtained when minimizing energy, FRD and degradation costs with two different battery sizes

| | Summer rates | | | | | | | | | | Winter rates | | | | | | | | | |
| | 80kWh battery | | | | | 40kWh battery | | | | | 80kWh battery | | | | | 40kWh battery | | | | |
Instance	Energy	Deg.	FRD	Total	Time (s)	Energy	Deg.	FRD	Total	Time (s)	Energy	Deg.	FRD	Total	Time (s)	Energy	Deg.	FRD	Total	Time (s)
1-3V	55.12	274.73	27.36	357.21	0.05	76.43	307.13	27.36	410.92	0.53	43.95	267.72	27.36	339.03	768.41	44.71	306.70	27.36	378.77	2.24
2-3V	50.67	269.86	27.36	347.89	0.05	71.59	297.60	27.36	396.55	0.20	42.70	261.62	27.36	331.68	4413.24	43.10	297.48	27.36	367.94	0.64
3-3V	55.76	281.75	27.36	364.87	0.05	74.56	313.42	27.36	415.34	0.19	44.70	272.21	27.36	344.27	81.27	44.84	313.42	27.36	385.62	0.61
4-3V	52.20	272.41	27.36	351.97	0.04	69.90	301.90	27.36	399.16	0.35	42.95	264.14	27.36	334.45	156.05	42.95	301.90	27.36	372.21	1.01
5-3V	46.01	275.29	27.36	348.66	0.06	66.82	304.19	27.36	398.37	0.19	42.51	265.14	27.36	335.01	355.49	42.60	303.54	27.36	373.50	1.49
1-6V	76.94	534.92	68.40	680.26	5.18	131.82	608.20	41.04	781.06	20.95	85.42	530.09	41.04	656.55	8176.51	85.84	605.84	41.04	732.72	74.16
2-6V	78.85	534.28	68.40	681.53	15.80	134.08	604.89	41.04	780.01	107.61	85.99	529.13	41.04	656.16	277.19	86.23	604.58	41.04	731.85	21.06
3-6V	75.91	539.95	68.40	684.26	3.63	137.21	606.35	41.04	784.60	10.21	85.85	529.82	41.04	656.71	1385.55	86.54	605.46	41.04	733.04	16.72
4-6V	76.69	544.58	68.40	689.67	4.23	138.76	618.29	41.04	798.09	58.34	87.21	537.54	41.04	665.79	160.92	87.94	617.64	41.04	746.62	14.49
5-6V	77.37	534.72	68.40	680.49	3.61	134.10	608.99	41.04	784.13	102.86	86.13	530.89	41.04	658.06	33.76	86.67	607.63	41.04	735.34	18.78
1-9V	128.81	813.96	82.08	1024.85	213.78	190.04	914.45	82.08	1186.57	18000.00	133.95	800.35	54.72	989.02	1508.82	133.61	914.91	54.72	1103.24	164.15
2-9V	127.88	815.66	82.08	1025.62	307.14	196.97	915.99	68.40	1181.36	36.10	134.23	799.55	54.72	988.50	218.70	133.56	918.47	54.72	1106.75	299.38
3-9V	132.93	814.71	82.08	1029.72	7372.71	197.32	918.02	82.08	1197.42	18000.00	135.06	802.14	54.72	991.92	338.02	129.75	917.40	68.40	1115.55	18000.00
4-9V	120.66	819.85	95.76	1036.27	541.93	191.25	931.07	82.08	1204.40	18000.00	134.84	810.92	54.72	1000.48	365.15	130.32	930.92	68.40	1129.64	18000.00
5-9V	120.25	826.23	95.76	1042.24	896.74	197.34	935.12	82.08	1214.54	18000.00	135.08	813.65	54.72	1003.45	1438.20	130.96	934.75	68.40	1134.11	18000.00

The results show that total costs are always lower with the larger battery, mostly because of savings in degradation costs. Since performing the routes with the smaller battery size requires larger discharge cycles, the batteries must be cycled in less preferable SOC intervals with regard to cyclic aging. With the summer rates the larger batttery size also allows for significant energy cost savings since more energy can be charged when it is cheap and stored for future use, whereas with the smaller battery size this is not always possible since each route requires discharging almost the entirety of the battery of the vehicle performing it. For example, as stated in Section 4.1, the vehicles in K_1 perform one route between 7:00 and 13:00 and another between 19:00 and 1:00 each day. With the larger battery size, these vehicles often leave for their first route with more energy than required since the peak rates between 12:00 and 18:00 are very high under the summer rates and routes only induce a SOC variation between 0.40 and 0.47. With the smaller battery, each route induces a SOC variation between 0.80 and 0.94, which makes it difficult for the vehicles in K_1 to store energy for their second route prior to leaving for their first route; more energy must thus

be charged during peak hours.

Whether or not these savings justify purchasing larger and more costly batteries should ultimately be determined based on a total cost of ownership analysis that takes into account the time-value of money, the projected number of battery replacements over the course of vehicle ownership, and the specific context at hand (and all its associated costs). The type of experiment conducted in this section can, however, help perform this analysis for different battery sizes and operational contexts since 1) its results can be used to assign values to operational costs that should be included in the total cost of ownership calculation (e.g., energy and FRD costs), and 2) the obtained degradation costs can be used to estimate the frequency of battery replacements by assuming a replacement will be required when the cumulative degradation costs of a battery reaches its purchase cost.

4.8 The impact of non-increasing cycling degradation costs

A significant benefit of the non-decreasing degradation costs of Table 7 used in all previous experiments is that cycling the battery in lower SOC intervals not only increases cycle life, but also indirectly benefits calendar life. This is, however, not the case when the battery wear function is non-increasing. Indeed, the cycle life data of some batteries may result in non-increasing cycling wear functions, suggesting that it would be preferable to avoid cycling such batteries in low SOC values, which would most likely lead to an increase in calendar aging. We illustrate this by solving the six-vehicle instances described in Section 4.1 with the winter rates of the TOU-EV-4 plan and the DOD cycle life data used in Hoke et al. (2011), which results in the non-increasing wear costs W_d reported in Table 17.

Table 17: Non-increasing battery degradation costs

SOC interval	Degradation costs
0–0.25	$0.19/kWh
0.25–0.5	$0.17/kWh
0.5–0.75	$0.13/kWh
0.75–1	$0.07/kWh

The results are reported in Table 18. The column "Avg. P. SOC" presents the average periodic SOC of the vehicles. In the determination of the average periodic SOC, it is assumed that the SOC decreases linearly from period to period while vehicles perform routes. The results presented in Table 18 show that calendar life is adversely affected when optimizing

the charging schedule with the non-increasing battery wear function from Table 17, since the average periodic SOC of the batteries is then significantly higher than the one obtained when optimizing without the wear costs. We therefore tried to mitigate calendar life losses resulting from the non-increasing wear cost function with the methodology proposed in Section 3.2 by minimizing the sum of the periodic SOC variables while allowing a maximum increase in total costs of 11% compared to those in the first phase solutions. The second phase solutions in Table 18 show that calendar aging can indeed be mitigated (since the average periodic SOC value decreases) while still ensuring smaller cycling degradation costs than those obtained when optimizing without the degradation costs, as well as similar energy and FRD costs to those obtained when optimizing with the degradation costs.

Table 18: Costs and average periodic SOC before and after mitigating calendar aging

	Solution without degradation costs				First phase solution with degradation costs					Second phase solution with degradation costs				
Instance	Energy	Deg.	FRD	Avg. P. SOC	Energy	Deg.	FRD	Avg. P. SOC	Time (s)	Energy	Deg.	FRD	Avg. P. SOC	Time (s)
1-6V	69.91	298.39	27.36	0.50	66.04	221.52	41.04	0.67	18000.00	67.09	256.63	41.04	0.55	18000.00
2-6V	70.20	289.27	27.36	0.52	65.80	220.71	41.04	0.68	18000.00	70.39	265.83	27.36	0.54	18000.00
3-6V	69.67	295.41	27.36	0.50	66.56	221.46	41.04	0.68	18000.00	68.25	255.97	41.04	0.55	18000.00
4-6V	71.41	293.65	27.36	0.51	66.98	223.26	41.04	0.68	18000.00	67.66	259.02	41.04	0.55	18000.00
5-6V	70.44	291.80	27.36	0.52	66.39	221.28	41.04	0.67	18000.00	70.60	266.90	27.36	0.54	18000.00

Moreover, Keil et al. (2016) have recently shown that the increase of calendar aging with SOC is not continuous but rather varies between a few SOC intervals (depending on the battery chemistry) within which calendar aging is similar. Figure 5 illustrates this by presenting the results of the accelerated calendar aging experiments conducted by Keil et al. (2016). As can be seen, even small reductions in the storage SOC can go a long way if it allows moving from a higher capacity fade plateau to a lower one, considering that the end of life of an electric vehicle battery is usually assumed to occur when its capacity has decreased to 80% of its initial value. Thus, assuming that the calendar aging incurred while a battery's SOC varies around an average SOC is similar to the calendar aging that would be incurred if the battery was only stored at that average SOC, the second phase solutions reported in Table 18 would significantly mitigate calendar aging for two of the three lithium-ion battery types presented in Figure 5 (i.e., NCA and NMC).

Finally, we mention that when optimizing energy, degradation and FRD costs with the non-decreasing wear costs (i.e., those in Table 7) used in all previous experiments, the average periodic SOC value obtained for the five instances of Table 18 is approximately 0.34. Jointly optimizing those degradation costs with the energy and FRD costs is therefore beneficial to both cycle life (as demonstrated in our previous experiments through the reduction of degra-
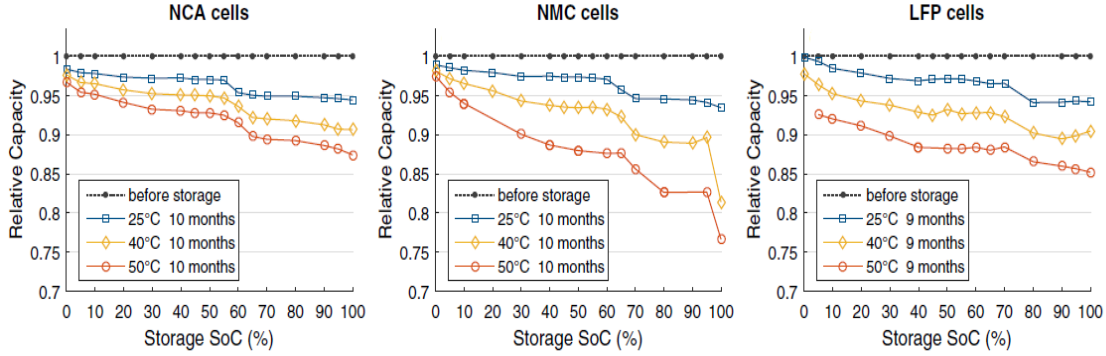
Figure 5: Results of accelerated calendar aging tests at various SOCs and temperatures
Source: Keil et al. (2016)

dation costs) and calendar life, since the average periodic SOC value decreases compared to the solutions obtained without degradation costs in Table 18.

5. Conclusions

The goal of this study was to develop and solve a comprehensive and practical mathematical model for depot charge scheduling that would integrate several useful considerations, as well as to derive managerial insights through computational experiments. The model can handle realistic charging functions, time-dependent energy costs, grid restrictions and FRD charges. We have also provided tractable methods for integrating an existing battery degradation function into the model. The tool can therefore be used to help the business case of EFVs operated in high use rate contexts by mitigating battery degradation occuring at a faster rate as a result of higher vehicle utilization, and by achieving the appropriate balance between energy and FRD costs.

Our numerical experiments suggest that degradation costs can indeed be mitigated by incurring slightly higher energy and FRD costs. We have also shown that when degradation costs are taken into account, the total costs can be decreased by splitting long routes into shorter ones with respect to SOC consumption. This modification allows more leeway regarding the selection of SOC intervals in which the battery is cycled. This may be of interest in operational contexts for which delivery routes stay relatively close to the depot so that vehicles can return to the depot more frequently, and where vehicles may be allowed perform evening or night-time deliveries so as to leave sufficient time for inter-route charging. Both of these operational characteristics are more likely to arise in the context where electric vehicles

37

are used for city logistics due to their limited range and silent operation.

We have shown that fees based on maximum charging powers can render the purchase of fast chargers solely for reducing energy costs unjustifiable in some contexts. However, such fast chargers may be required for vehicle operation flexibility when longer routes are performed. Moreover, we have demonstrated how the model may be used to compare different plans offering tradeoffs between grid restrictions, energy costs, FRD charges, and fixed customer charges. **In the same vein, the model can help compare achievable costs with different battery sizes.** We have also concluded that depending on the nature of the cycling wear function (i.e., depending on the battery), the integration of calendar aging considerations becomes less critical. If the cycling wear cost function increases with the SOC, then even without calendar aging mitigation, the joint optimization of energy, FRD and degradation costs is beneficial to both the cycle and calendar lifetime of the batteries. However, if the cycling wear cost function decreases with the SOC, our results suggest that additional steps may be required to mitigate calendar aging in order to avoid spending lengthy periods of time at high SOC values. We have therefore provided a simple methodology to this end.

Finally, we believe that interesting research avenues lie in the integration of some of the methods discussed in this paper into other problem settings. These may include simultaneously optimizing the charging schedule and assigning vehicles to routes, or even simultaneously routing the vehicles, both of which would require the development of heuristics. Moreover, the proposed methodology for incorporating cycling wear costs is applicable to any electric vehicle routing problem with en route partial recharging, and could thus be used to investigate the impact of such wear costs on solutions of these problems, e.g., it may induce more frequent stops at charging stations in order to cycle the batteries in the SOC intervals with the lowest wear costs.

Acknowledgements

Appendix A. Glossary of abbreviations

A: Ampere.

Ah: Ampere-hour.

ACC-DOD: Achievable cycle count as a function of DOD.

CC-CV: Constant current-constant voltage.

DOD: Depth of discharge.

EFV : Electric freight vehicle.

FRD charges: Facility-related demand charges.

kW: Kilowatt.

kWh: Kilowatt-hour.

SOC: State of charge.

V: Volt.

Appendix B. Incorporating general wear cost functions

Since the wear cost is constant in a given SOC interval, a cumulative wear cost function can be represented as a piecewise linear function of SOC regardless of the shape of the wear cost function. A point at a given SOC in this cumulative wear cost function would indicate the total wear costs incurred for charging the battery from 0 to that SOC. The idea is essentially to determine initial and final positions on a piecewise linear function by constructing convex combinations of the function's breakpoints. **As for non-increasing wear cost functions with respect to SOC, with a general wear cost function, some energy could be charged that will never be discharged in an EFV-CSP optimal solution. We must therefore monitor the amount of energy charged and discharged in each SOC interval of the degradation model separately in order to incorporate both charging and discharging cyclic degradation. For the sake of brevity, we only provide a formulation to incorporate the cyclic aging incurred during charging for general wear cost functions, however the cyclic aging incurred during discharging can be incorporated in a very similar fashion.**

Let ζ_{dr} be a binary variable equal to 1 if and only if the SOC of vehicle v_r lies between $\overline{S}_{d-1}$ and $\overline{S}_d$ upon arriving from route η_r or at the start of the horizon if $r = f_{v_r}$, with $\overline{S}_0 = \underline{S}_1$. Similarly, let ψ_{dr} be a binary variable equal to 1 if and only if the SOC of vehicle v_r lies between $\overline{S}_{d-1}$ and $\overline{S}_d$ upon leaving for route r. Let ϵ_{dr} and w_{dr} be the coefficients of

breakpoint $\overline{S}_d$ used in the convex combinations to determine the position of vehicle v_r on the cumulative wear function when arriving from η_r (or the start of the horizon if $r = f_{v_r}$) and leaving for r respectively. Let cs_r and ce_r be the starting and ending cost positions of vehicle v_r on the cumulative wear function when arriving from η_r (or the start of the horizon if $r = f_{v_r}$) and leaving for r respectively. Let C_d be the cumulative wear cost in the piecewise linear function at breakpoint $\overline{S}_d$, for all $d \in D \cup \{0\}$. Then any discrete wear cost function can be incorporated into the EFV-CSP by means of the following constraints:

$$\sum_{d \in D \cup \{0\}} \epsilon_{dr} = \sum_{d \in D} \zeta_{dr} = 1 \quad r \in R \tag{31}$$

$$\sum_{d \in D \cup \{0\}} w_{dr} = \sum_{d \in D} \psi_{dr} = 1 \quad r \in R \tag{32}$$

$$soc_{\alpha_{\eta_r}, v_r} = \sum_{d \in D \cup \{0\}} \epsilon_{dr} \cdot \overline{S}_d \quad r \in R \tag{33}$$

$$soc_{\beta_r, v_r} = \sum_{d \in D \cup \{0\}} w_{dr} \cdot \overline{S}_d \quad r \in R \tag{34}$$

$$cs_r = \sum_{d \in D \cup \{0\}} \epsilon_{dr} \cdot C_d \quad r \in R \tag{35}$$

$$ce_r = \sum_{d \in D \cup \{0\}} w_{dr} \cdot C_d \quad r \in R \tag{36}$$

$$\epsilon_{0r} \leq \zeta_{1r} \quad r \in R \tag{37}$$

$$\epsilon_{dr} \leq \zeta_{dr} + \zeta_{d+1,r} \quad d \in D \backslash \{n_d\}, r \in R \tag{38}$$

$$\epsilon_{n_d,r} \leq \zeta_{n_d,r} \quad r \in R \tag{39}$$

$$w_{0r} \leq \psi_{1r} \quad r \in R \tag{40}$$

$$w_{dr} \leq \psi_{dr} + \psi_{d+1,r} \quad d \in D \backslash \{n_d\}, r \in R \tag{41}$$

$$w_{n_d,r} \leq \psi_{n_d,r} \quad r \in R \tag{42}$$

$$\zeta_{dr}, \psi_{dr} \in \{0, 1\} \quad d \in D, r \in R \tag{43}$$

$$\epsilon_{dr}, w_{dr} \geq 0 \quad d \in D \cup \{0\}, r \in R. \tag{44}$$

Constraints (31)–(32) ensure that the SOC values upon arriving from a route (or at the start of the horizon) and leaving for the next route to be between two of the SOC breakpoints of the cumulative wear function, and force the sum of the breakpoint coefficients to be equal

to 1. Constraints (31)–(34) and (44) together force the SOC values upon arriving from a route (or at the start of the horizon) and leaving for the next route to be convex combinations of the SOC breakpoints of the cumulative wear cost function. Constraints (35)–(36) determine the costs on the cumulative wear function corresponding to these convex combinations. Constraints (37)–(42) force these convex combinations to only use two consecutive breakpoints of the cumulative wear cost function. Constraints (43)–(44) define the domains of the new variables. Finally, in this case, the objective function (2) should be replaced with

$$\text{minimize} \quad \sum_{k \in K} \sum_{p \in P} c_p \cdot E \cdot \frac{\delta \cdot i_{pk}}{Q} + F \cdot y + \sum_{r \in R} (ce_r - cs_r). \tag{45}$$

References

Afroditi, A., M. Boile, S. Theofanis, E. Sdoukopoulos, D. Margaritis. 2014. Electric vehicle routing problem with industry constraints: trends and insights for future research. *Transportation Research Procedia* **3** 452–459.

Barré, A., B. Deguilhem, S. Grolleau, M. Gérard, F. Suard, D. Riu. 2013. A review on lithium-ion battery ageing mechanisms and estimations for automotive applications. *Journal of Power Sources* **241** 680–689.

Bashash, S., S.J. Moura, J.C. Forman, H.K. Fathy. 2011. Plug-in hybrid electric vehicle charge pattern optimization for energy cost and battery longevity. *Journal of Power Sources* **196** 541–549.

Bruglieri, M., F. Pezzella, O. Pisacane, S. Suraci. 2015. A variable neighborhood search branching for the electric vehicle routing problem with time windows. *Electronic Notes in Discrete Mathematics* **47** 221–228.

Conrad, R.G., M.A. Figliozzi. 2011. The recharging vehicle routing problem. In: Doolen, T., Van Aken, E. (Eds.), *Proceedings of the 2011 Industrial Engineering Research Conference* (IISE, Norcross, GA), 2785–2792.

Davis, B.A., M.A. Figliozzi. 2013. A methodology to evaluate the competitiveness of electric delivery trucks. *Transportation Research Part E* **49**(1) 8–23.

eMotorWerks. 2017. JuiceBox EV charging stations. URL `https://emotorwerks.com/products/juicebox`. Last accessed 6/6/2017.

E-Mobility NSR. 2013. Comparative analysis of european examples of schemes for freight electric vehicles - compilation report. E-Mobility NSR, Aalborg, Denmark. URL `http://e-mobility-nsr.eu/fileadmin/user_upload/downloads/info-pool/E-Mobility_-_Final_report_7.3.pdf`. Last accessed 15/6/2017.

Felipe, Á., M.T. Ortuño, G. Righini, G. Tirado. 2014. A heuristic approach for the green vehicle routing problem with multiple technologies and partial recharges. *Transportation Research Part E* **71** 111–128.

Feng, W., M. Figliozzi. 2013. An economic and technological analysis of the key factors affecting the competitiveness of electric commercial vehicles: a case study from the USA market. *Transportation Research Part C* **26** 135–145.

Franceschetti, A.,D. Honhon, G. Laporte, T. Van Woensel, J.C. Fransoo. 2017. Strategic fleet planning for city logistics. *Transportation Research Part B* **95** 19–40.

Goeke, D., M. Schneider. 2015. Routing a mixed fleet of electric and conventional vehicles. *European Journal of Operational Research* **245**(1) 81–99.

Han, S., S. Han, H. Aki. 2014. A practical battery wear model for electric vehicle charging applications. *Applied Energy* **113** 1100–1108.

Hiermann, G., J. Puchinger, S. Ropke, R.F. Hartl. 2016. The electric fleet size and mix vehicle routing problem with time windows and recharging stations. *European Journal of Operational Research* **252**(3) 995–1018.

Hoke, A., A. Brissette, D. Maksimović, A. Pratt, I. Labs, K. Smith. 2011. Electric vehicle charge optimization including effects of lithium-ion battery degradation. *2011 IEEE Vehicle Power and Propulsion Conference* (IEEE, Piscataway, NJ), 1–8.

Keil, P., S.F. Schuster, J. Wilhelm, J. Travi, A. Hauser, R.C. Karl, A. Jossen. 2016. Calendar aging of lithium-ion batteries – I. Impact of the graphite anode on capacity fade. *Journal of The Electrochemical Society* **163**(9) A1872–A1880.

Kovacs, A.A., B.L. Golden, R.F. Hartl, S.N. Parragh. 2014. Vehicle routing problems in which consistency considerations are important: a survey. *Networks* **64**(3) 192–213.

Lam, L. 2011. A practical circuit-based model for state of health estimation of li-on battery cells in electric vehicles. Master's thesis, Delft University of Technology, Delft, The Netherlands.

Lebeau, P., C. De Cauwer, J. Van Mierlo, C. Macharis, W. Verbeke, T. Coosemans. 2015. Conventional, hybrid, or electric vehicles: which technology for an urban distribution centre? *The Scientific World Journal*, Article ID 302867.

Lee, D.Y., V.M. Thomas, M.A. Brown. 2013. Electric urban delivery trucks: energy use, greenhouse gas emissions, and cost-effectiveness. *Environmental Science & Technology* **47**(14) 8022–8030.

Lunz, B., Z. Yan, J.B. Gerschler, D.U. Sauer. 2012. Influence of plug-in hybrid electric vehicle charging strategies on charging and battery degradation costs. *Energy Policy* **46** 511–519.

Marra, F., G.Y. Yang, C. Traholt, E. Larsen, C.N. Rasmussen, S. You. 2012. Demand profile study of battery electric vehicle under different charging options. *2012 IEEE Power and Energy Society General Meeting* (IEEE, Piscataway, NJ), 3428–3434.

Montoya, A., C. Guéret, J.E. Mendoza, J.G. Villegas. 2017. The electric vehicle routing problem with nonlinear charging function. *Transportation Research Part B* **103** 87–110.

Morganti, E., M. Browne. 2018. Technical and operational obstacles to the adoption of electric vans in France and the UK: an operator perspective. *Transport Policy* **63** 90–97.

Naberezhnykh, D., J J. Wardle, J J. Lowes, C. Herron, T. Brightman, T. Parker. 2012. Electric vehicle charging points for freight vehicles in central London. Prepared for Central London FQP by Transport & Travel Research Ltd, in partnership with TRL and Zero Carbon Futures. URL `http://www.centrallondonfqp.org/app/download/12240926/CLFQP_EVCP_strategy+report_Final+v1+0.pdf`. Last accessed 15/6/2017.

Nesterova, N., H. Quak, S. Balm, I. Roche-Cerasi, T. Tretvik. 2013. Project FREVUE deliverable D1.3: state of the art of the electric freight vehicles implementation in city logistics. TNO and SINTEF. European Commission Seventh Framework Programme.

Nykvist, B., M. Nilsson. 2015. Rapidly falling costs of battery packs for electric vehicles. *Nature Climate Change* **5** 329–332.

Pelletier, S., O. Jabali, G. Laporte. 2016. 50th anniversary invited article - Goods distribution with electric vehicles: review and research perspectives. *Transportation Science* **50**(1) 3–22.

Pelletier, S., O. Jabali, G. Laporte, M. Veneroni. 2017. Battery degradation and behaviour for electric vehicles: review and numerical analyses of several models. *Transportation Research Part B* **103** 158–187.

Preis, H., S. Frank, K. Nachtigall. 2014. Energy-optimized routing of electric vehicles in urban delivery systems. In: Helber, S., Breitner, M., Rösch, D., Schön, C. Graf von der Schulenburg, J-M., Sibbertsen, P., Steinbach, M., Weber, S., Wolter, A. (Eds.), *Operations Research Proceedings 2012* (Springer International Publishing, Switzerland), 583–588.

Quak, H., N. Nesterova, T. van Rooijen. 2016. Possibilities and barriers for using electric-powered vehicles in city logistics practice. *Transportation Research Procedia* **12** 157–169.

Sassi, O., A. Oulamara. 2014a. Joint scheduling and optimal charging of electric vehicles problem. In: Murgante, B., Misra, S., Rocha, A.M.A.C., Torre, C., Rocha, J.G., Falcão, M.I., Taniar, D., Apduhan, B.O., Gervasi, O. (Eds.), *ICCSA 2014 Proceedings, Part II*. Lecture Notes in Computer Science, vol. 8580 (Springer International Publishing, Switzerland), 76-91.

Sassi, O., A. Oulamara. 2014b. Simultaneous electric vehicles scheduling and optimal charging in the business context: case study. *5th IET Hybrid and Electric Vehicles Conference* (IET, Stevenage, UK), 105–110.

Schiffer, M., G. Walther. 2017a. An adaptive large neighborhood search for the location routing problem with intraroute facilities. *Transportation Science*, Articles in Advance. doi:10.1287/trsc.2017.0746.

Schiffer, M., G. Walther. 2017b. The electric location routing problem with time windows and partial recharging. *European Journal of Operational Research* **260**(3) 995–1013.

Schiffer, M., G. Walther. 2017c. Strategic planning of electric logistics networks: a robust location routing approach. *Omega*. doi:10.1016/j.omega.2017.09.003. In Press.

Schiffer, M., M. Schneider, G. Laporte. 2018. Designing sustainable mid-haul logistics networks with intra-route multi-resource facilities. *European Journal of Operational Research* **265**(2) 517–532.

Schneider, M., A. Stenger, D. Goeke. 2014. The electric vehicle-routing problem with time windows and recharging stations. *Transportation Science* **48**(4) 500–520.

Shareef, H., M.M. Islam, A. Mohamed. 2016. A review of the state-of-the-art charging technologies, placement methodologies, and impacts of electric vehicles. *Renewable and Sustainable Energy Reviews* **64** 403–420.

Southern California Edison. 2017. Electric car rate options. URL `sce.com/wps/portal/home/business/rates/electric-car-business-rates`. Last accessed 6/6/2017.

Taefi, T.T. 2016. Viability of electric vehicles in combined day and night delivery: a total cost of ownership example in Germany. *European Journal of Transport and Infrastructure Research* **16**(4) 600–618.

Taefi, T.T., S. Stütz, A. Fink. 2016. Increasing the mileage of battery electric medium duty vehicles: a recipe for competitiveness? Helmut-Schmidt University Hamburg, Institute of Computer Science Research Paper Series, Research Paper 16–01.

Tremblay, O., L.-A. Dessaint, A.-I. Dekkiche. 2007. A generic battery model for the dynamic simulation of hybrid electric vehicles. *2007 Vehicle Power and Propulsion Conference* (IEEE, Piscataway, NJ), 284–289.

Yang, J., H. Sun. 2015. Battery swap station location-routing problem with capacitated electric vehicles. *Computers & Operations Research* **28** 217–232.